Marcks and Marcks-like 1 proteins promote spinal cord development and regeneration in *Xenopus*

Mohamed El Amri[1,2], Abhay Pandit[2], Gerhard Schlosser[1]*

[1]School of Biological and Chemical Sciences, University of Galway, Biomedical Sciences Building, Newcastle Road, Galway H91 W2TY, Ireland

[2]SFI Research Centre for Medical Devices (CÚRAM), University of Galway, Biomedical Sciences Building, Newcastle Road, Galway H91 W2TY, Ireland

***Corresponding author**:
School of Biological and Chemical Sciences, University of Galway, Biomedical Sciences Building, Newcastle Road, Galway H91 W2TY, Ireland, Phone: 00353-91-495978, E-mail: gerhard.schlosser@universityofgalway.ie

Abstract

Marcks and Marcksl1 are abundant proteins that shuttle between the cytoplasm and membrane to modulate multiple cellular processes, including cytoskeletal dynamics, proliferation, and secretion. Here, we performed loss- and gain-of-function experiments in *Xenopus laevis* to reveal the novel roles of these proteins in spinal cord development and regeneration. We show that Marcks and Marcksl1 have partly redundant functions and are required for normal neurite outgrowth and proliferation of neuro-glial progenitors during embryonic spinal cord development and for its regeneration during tadpole stages. Rescue experiments in Marcks and Marcksl1 knockout animals further suggested that some of the functions of Marcks and Marcksl1 in the spinal cord are mediated by phospholipase D (PLD) signaling. Taken together, these findings identify Marcks and Marcksl1 as critical new players in spinal cord development and regeneration and suggest new pathways to be targeted for therapeutic stimulation of spinal cord regeneration in human patients.

Introduction

Spinal cord injury in humans is a life-changing condition with no effective treatment. However, many non-mammalian vertebrates can fully regenerate their spinal cords after injury (Lee-Liu, Edwards-Faret, Tapia, & Larrain, 2013, Alunni & Bally-Cuif, 2016, Rodemer, Hu, Selzer, & Shifman, 2020). In the clawed toad *Xenopus*, tadpoles can fully regenerate the spinal cord; however, this capacity is lost during metamorphosis (Beattie, Bresnahan, & Lopate, 1990, Gibbs, Chittur, & Szaro, 2011). Therefore, *Xenopus* offers a rare opportunity to compare cellular and molecular responses to spinal cord injury (SCI) in a regeneration-competent system with a regeneration-incompetent system in the same species. Thus, differences between the responses to SCI in the two stages likely have some functional implications for the difference in regenerative capacity rather than reflecting other phylogenetically accumulated differences in development, as may be the case when different species are compared.

A recent proteomic screen to identify proteins differentially regulated in regeneration-competent tadpoles versus regeneration-incompetent froglets after SCI identified Marcks and Marcksl1 as proteins that are highly upregulated at the tadpole stage but downregulated in froglets (Kshirsagar, 2020), suggesting a potential role for these proteins in spinal cord regeneration.

Marcks is an abundant and widely expressed protein with three highly conserved functional domains: an effector domain (ED), a Marcks Homology 2 (MH2) domain, and a myristoylation domain (Brudvig & Weimer, 2015, El Amri, Fitzgerald, & Schlosser, 2018). Marcks-like protein 1 (Marcksl1) shares strong homology and functionality with Marcks (Stumpo et al., 1998). In an unphosphorylated state, the positively charged ED of Marcks attaches to the plasma membrane, and the myristoylation site tethers the protein to the membrane (Kim, Blackshear, Johnson, & McLaughlin, 1994, McLaughlin & Aderem, 1995). However, when the ED is phosphorylated by Protein kinase C (PKC), thereby acquiring more negative charges, Marcks translocates to the cytoplasm (Brudvig & Weimer, 2015; McLaughlin & Aderem, 1995).

Depending on their phosphorylation status and subcellular localization, Marcks and Marcksl1 regulate multiple processes in the cell. For example, they have been shown to modulate the polymerization and cross-linking of actin filaments, recruit secretory vesicles to the embrane, and interact with phosphatidylinositol 4,5-bisphosphate (PIP_2), thereby regulating multiple signaling pathways downstream of PIP_2 such as phospholipase C (PLC)

and phospholipase D (PLD) dependent pathways (Hartwig et al., 1992, Morash, Rose, Byers, Ridgway, & Cook, 1998, Yarmola, Edison, Lenox, & Bubb, 2001, Wohnsland, Schmitz, Steinmetz, Aebi, & Vergeres, 2000, McLaughlin, Wang, Gambhir, & Murray, 2002, Sundaram, Cook, & Byers, 2004, Xu et al., 2014). Consequently, Marcks and Marcksl1 affect cytoskeletal dynamics, cell migration, secretion, cell proliferation, and differentiation in the nervous system and other tissues (Brudvig & Weimer, 2015, El Amri et al., 2018).

Importantly, Marcks and Marcksl1 proteins were found to be upregulated in several different regenerative processes, such as lens regeneration in newts, fin regeneration in lungfish and bichirs, tail regeneration in lizards, and cardiac tissue regeneration following infarction in mice (Bock-Marquette et al., 2009, Sousounis et al., 2014, Nogueira et al., 2016, Alibardi, 2017, Lu et al., 2019). Moreover, a Marcks- and Marcksl1-like protein in axolotls (AxMLP) initiates an early proliferative response in axolotl tail and limb regeneration (Sugiura, Wang, Barsacchi, Simon, & Tanaka, 2016). In the nervous system, Marcks and Marcksl1 are also significantly upregulated in outgrowing and/or regenerating neurites of facial motor neurons, dorsal root and superior cervical ganglia, in the optic nerve and during axonal sprouting after brain stroke, suggesting an essential role for Marcks and Marcksl1 in neurite outgrowth and regeneration in both the peripheral and central nervous systems (McNamara, Jiang, Streit, & Lenox, 2000, Carmichael et al., 2005, Szpara et al., 2007, Veldman, Bemben, Thompson, & Goldman, 2007).

In this study, we combined Marcks and Marcksl1 gain- and loss-of-function experiments in *Xenopus laevis* with histological and behavioral analyses to show, for the first time, that Marcks and Marcksl1 also play essential roles during spinal cord development and regeneration. We demonstrate that both proteins have partly redundant functions and are required for normal neurite outgrowth and the proliferation of neuro-glial progenitors during the development of the spinal cord, as well as for its regeneration after full transection. Rescue experiments with pharmacological compounds in Marcks and Marcksl1 knockout animals further suggest that at least some of the functions of Marcks and Marcksl1 in the spinal cord are mediated by PLD signaling. Taken together, these findings identify Marcks and Marcksl1 as critical new players in spinal cord development and regeneration and highlight the power of *Xenopus* as an experimental model for identifying new pathways required for regeneration competence.

Results

Marcks and Marcksl1 are expressed in the developing Xenopus spinal cord

To elucidate the role of Marcks and Marcksl1 for spinal cord development, we first analyzed mRNA expression of *marcks.S*, *marcksl1.S*, and *marcksl1.L* in embryos of *Xenopus laevis* at stages 26 and 34 (early and late tailbud stage, respectively). Due to the 94% sequence identity between *marcks.S* and *marcks.L* mRNAs, the *marcks.S* probe is expected to cross-react with *marcks.L*, while *marcksl1.S* and *marcksl1.L* mRNA have only 84% identity and show slightly different expression suggesting that they exhibit only limited if any cross-reactivity. Whole-mount in situ hybridization showed that all of these genes have a similar pattern of expression (Fig. 1 A-G, Fig. S1). They are strongly expressed in the brain and spinal cord as well as in the pharyngeal arches, somites, intermediate mesoderm, and blood islands of the ventrolateral mesoderm. *marcks*.S is more broadly distributed through the entire brain, whereas *marcksl1.L* and *marcksl1.S* have a more restricted expression and are absent from the forebrain. Vibratome sections of stage 34 embryos after whole-mount in situ hybridization confirmed the expression of all genes throughout the spinal cord as well as in the brain, lens, pharyngeal arches, somites, and other mesodermal derivatives (Fig. 1 H, I; Fig. S2-4). They also reveal the expression of all genes in the epidermis and of *marcks.S* in the otic vesicle and show that *marcksl1.S* has a weaker and more restricted expression in the brain and spinal cord than *marcksl1.L*.

We next used two polyclonal antibodies raised against epitopes shared between *Xenopus laevis* Marcks.S and Marcks.L protein and between Marcksl1.S and Marcksl1.L, respectively, to clarify the subcellular distribution of Marcks and Marcksl1 proteins in the developing spinal cord. These antibodies specifically recognize Marcks and Marcksl1 proteins, respectively, without cross-reactivity (Fig. S5). Confocal microscopy of embryos injected with mRNAs encoding a membrane-tethered form of GFP (*memGFP*) and transversely sectioned at stage 26 revealed that Marcks and Marcksl1 are mostly associated with outer cell membranes. This is true for the ventricular zone, where progenitor cells are located, and the adjacent mantle zone, which harbors migrating and differentiating neurons (Fig. 1 K-P). In addition, a subset of cells in both ventricular and mantle zones shows cytoplasmic expression of Marcks and Marcksl1. Marcks, but not Marcksl1 was also occasionally seen in cell nuclei.

Because shuttling between the membrane and cytoplasm is essential for the function of Marcks and Marcksl1 in other developmental contexts (El Amri et al., 2018), their subcellular localization to membranes and cytoplasm in the spinal cord and their widespread distribution in the developing spinal cord suggests that these proteins may play hitherto unrecognized

roles during normal spinal cord development. To test this hypothesis, we next used two independent approaches, injection of antisense Morpholino oligonucleotides (MO) and CRISPR/Cas9- mediated gene editing, to determine how knockdown/-out of these proteins affects neurite outgrowth, cell proliferation, and neuro-glial progenitor populations during spinal cord development.

Marcks and Marcksl1 are required for normal neurite outgrowth during spinal cord development

We first studied the role of Marcks and Marcksl1 in neurite outgrowth in the spinal cord individually by injecting a single blastomere in 4-to-8-cell stage embryos with either an MO blocking the translation of both *marcks.L* and *marcks.S* or with a mixture of two MOs blocking the translation of *marcksl1.L* and *marcksl1.S,* respectively. This resulted in the unilateral knockdown of the respective proteins on the injected side of the embryo, whereas the uninjected side developed normally. *myc-GFP* mRNA was co-injected to identify the injected side. The effectiveness and specificity of all MOs used were validated by in vitro transcription and translation of the various proteins in the presence or absence of the appropriate MO (Fig. S6). None of these injections led to significant alterations in immunostaining for the neurite marker acetylated tubulin on the injected side of the spinal cord relative to the uninjected side in stage 34 embryos compared to an unspecific control MO (Fig. 2 A-C). However, when the three MOs targeting *marcks.S/L*, *marcksl1.S,* and *marcksl1.L* were co-injected, thus blocking all four homeologs (4M MO), acetylated tubulin staining was significantly decreased on the injected side (Fig. 2, D, E, G). Co-injection of mRNA constructs encoding chicken Marcks and *Xenopus tropicalis* Marcksl1, which were selectively mutated to prevent MO binding, resulted in complete rescue of acetylated tubulin staining, confirming the specific action of the MOs used (Fig. 2 F, G). This suggests that Marcks and Marcksl1 are required for neurite outgrowth during spinal cord development but act in a largely redundant fashion. To account for these overlapping functions, we aimed to simultaneously knockdown or knockout all four proteins (Marcks.L/S, Marcksl1.L/S) for the rest of our study.

To verify the results of our MO knockdown experiments, we analyzed F0 embryos after CRISPR-Cas9 gene editing. For these experiments, single-guide RNA constructs targeting *marcks.S*, *marcks.L*, *marcksl1.S,* and *marcksl1.L* genes were co-injected with Cas9 as a ribonucleoprotein (RNP) and *myc-GFP* mRNA into one blastomere during the 1-cell stage

for genotyping or the 4-to-8 cell stage for phenotypic analysis. At later embryonic stages (stage 26-42), genomic DNA was extracted from some of the embryos, sequenced, and analyzed with Synthego Inference for CRISPR Edits (ICE) to determine the frequency with which indels were generated in the targeted region (indel score) as well as the frequency of indels with frameshifts (knockout score). Sibling embryos were used for phenotypic analysis. In control experiments, we either injected Cas9 protein and *myc-GFP* mRNA alone or injected a sgRNA targeting *slc45a2* (DeLay et al., 2018), encoding a protein that mediates melanin synthesis, Cas9 proteins, and *myc-GFP* mRNA. When analyzing CRISPR/Cas9 edited animals in the F0 generation, a considerable and variable extent of mosaicism has to be taken into account because different gene editing events may occur in different subsets of cells (Blitz, Biesinger, Xie, & Cho, 2013; DeLay et al., 2018). We, therefore, first tested a range of different sgRNAs to ensure high overall gene editing and knockout efficiencies.

We first validated our CRISPR knockout procedure using the control gene *slc45a2*. Embryos injected during the 1-cell stage with *slc45a2* RNPs and analyzed at stages 37-46 lost pigmentation in both eyes, whereas embryos injected during the 2-to-4-cell stage showed loss of pigmentation only in the injected side. Confirming a previous report (DeLay et al., 2018), genomic sequencing revealed a high indel score (93%) and knockout score (67-68%) in these embryos (Fig. S7). Almost all surviving embryos displayed visible oculocutaneous albinism, with the majority showing almost no eye pigment (Fig. S7).

Next, we designed, synthesized, and tested a total of 18 sgRNA transcripts targeting either *marcks.L/S* or *marcksl1.L/S* (sgRNAs were designed to target both homeologs of each gene) and selected the sgRNA transcripts creating the highest and most consistent number of indels and knockout scores for each pair of genes - named *marcks.L/S* and *marcksl1.L/S* sgRNA, respectively - for further experiments (Figs. S8-11). The *marcks.L/S* sgRNA introduced indels in 88% of the targeted DNA from *marcks.L* exon 1 (8 embryos) and 84% from *marcks.S* exon 1 (8 embryos), with an average of 78% and 76%, respectively, consisting of frameshift mutations which may contribute to a functional knockout (Figs. S8 C, S9 C). The *marcksl1.L/S* sgRNA introduced indels in 73% of the targeted DNA from *marcksl1.L* exon 2 (6 embryos) and 73% from *marcksl1.S* exon 2 (7 embryos), with an average of 50% and 47%, respectively, being out-of-frame (Figs. S10 C, S11 C). We also confirmed by immunohistochemistry that co-injection of *marcks.L/S* and *marcksl1.L/S* sgRNA, which is predicted to edit all four homeologs (henceforth denoted as 4M CRISPR) drastically reduced immunostaining for Marcks and Marcksl1 protein on the injected side (Fig. S6 B-G), indicating that protein levels are reduced in gene-edited embryos.

Similar to the knockdown of the proteins by MOs, the unilateral CRISPR-mediated knockout of all Marcks and Marcksl1 homeologs (4M CRISPR) led to a significant reduction in acetylated tubulin staining on the injected side compared to Cas9 and *slc45a2* controls (Fig. 2 H-K). Conversely, overexpression of both proteins by injection of *marcks* and *marcksl1* mRNA at two different doses (100 or 300 pg each) together with *myc-GFP* mRNA resulted in a significant increase in acetylated tubulin staining on the injected side compared to that in control embryos injected with *myc-GFP* mRNA alone (Fig. S12). Taken together; these results suggest that Marcks and Marcksl1 play essential roles for neurite outgrowth during normal embryonic development of the *Xenopus* spinal cord, with elevated levels of Marcks and Marcksl1 being able to further promote neurite outgrowth.

Marcks and Marcksl1 are required for the proliferation of neuro-glial progenitors during spinal cord development

Next, we tested whether Marcks and Marcksl1 are required for the proliferation of neuro-glial progenitor cells during spinal cord development. After unilateral injection with a cocktail of the three MOs targeting *marcks.S/L*, *marcksl1.S* and *marcksl1.L* (4M MO) or with the combined *marcks.L/S* and *marcksl1.L/S* sgRNAs (4M CRISPR), we analyzed the number of cells in mitosis in the spinal cord of stage 34 embryos by immunostaining against phospho-histone H-3 (PH3). In both control and experimental animals, PH3-positive nuclei are confined to the ventricular zone at this stage, where neuro-glial progenitors reside (Fig. 3 A-C, E-G). The proportion of PH3-positive ventricular nuclei on the injected side (expressed as the ratio between injected/uninjected sides) was significantly reduced in both experiments compared to control injections (Fig. 3 A-H). Conversely, the injection of *marcks* and *marcksl1* mRNA together with *myc-GFP* mRNA resulted in a significant increase in the proportion of PH3-positive ventricular nuclei on the injected side compared to control embryos injected with *myc-GFP* mRNA alone (Fig. S13). These observations indicate that Marcks and Marcksl1 are required for normal patterns of cell proliferation in the ventricular zone of the developing spinal cord. In addition, increased levels of Marcks and Marcksl1 are sufficient to further promote cell proliferation.

To directly test the role of Marcks and Marcksl1 for neuro-glial progenitors, we next immunostained spinal cords of stage 34 embryos for the progenitor markers Sox2 or Sox3 after unilateral injection of *marcks.L/S* and *marcksl1.L/S* sgRNAs. The numbers of Sox2- or Sox3-positive nuclei on the injected side (expressed as a ratio between injected/uninjected

sides) was significantly reduced as compared to control embryos injected with *slc45a2* sgRNAs or with Cas9 alone (Fig. 3 I-M). This indicates that Marcks and Marcksl1 are required for maintaining a normal pool of neuro-glial progenitor cells during spinal cord development. This may at least partly result from the role of both proteins in promoting the proliferation of these neuro-glial progenitors, as described above, but additional roles for the survival and maintenance of neuro-glial progenitors cannot be ruled out.

PLD and other signaling pathways mediate the functions of Marcks and Marcksl1 during spinal cord development

Since Marcks and Marcksl1 are known to be multifunctional proteins, we next asked which signaling pathways may mediate the effects of Marcks and Marcksl1 during spinal cord development. Our experiments described so far suggested essential functions of these proteins in both proliferation control and neurite outgrowth. We, therefore, focused on the phospholipase D (PLD) dependent signaling pathway since previous studies have suggested that PLD signaling is activated downstream of Marcks (Morash, Byers, & Cook, 2000; Morash et al., 1998) and has essential functions in both the regulation of mitosis and of cytoskeletal dynamics including neurite outgrowth (Kam & Exton, 2001, Foster & Xu, 2003, Zhang et al., 2004, Brown, Thomas, & Lindsley, 2017). To activate and inhibit PLD signaling, we used Sphingosine-1-phosphate (S1P) and 5-Fluoro-2-indolyl des-chlorohalopemide (FIPI), dissolved in 2% DMSO, respectively (Meacci et al., 2003, Monovich et al., 2007, Su et al., 2009).

Embryos were unilaterally injected with *marcks.L/S* and *marcksl1.L/S* sgRNAs (4M CRISPR), as described above, were then raised for one day before fixation in PLD activators or inhibitors and were analyzed at stage 34 by immunostaining for the neurite marker acetylated tubulin and the mitosis marker PH3. 4M CRISPR-injected control embryos were raised in 2% DMSO and similarly analyzed. Compared to DMSO-treated controls, incubation in the PLD activator S1P significantly increased the intensity of acetylated tubulin staining (Fig. 4 A) as well as the proportion of PH3-positive cells (Fig. 4 B) on the CRISPR-injected side relative to the uninjected side, whereas the PLD inhibitor FIPI had no significant effect (Fig. 4 A, B). The ability of PLD activation but not inhibition to rescue the deficiencies in the CRISPR-injected embryos suggests that Marcks and Marcksl1 promote neurite outgrowth and progenitor proliferation at least partly by a PLD-dependent mechanism.

Because PLD signaling downstream of Marcks has previously been suggested to be PIP_2 dependent (Morash et al., 2000; Sundaram et al., 2004), we next tested whether enhancement or inhibition of PIP_2 synthesis is also able to modulate the effects on spinal cord development in our CRISPR-injected embryos. For PIP_2 biosynthesis enhancement and inhibition, we incubated 4M CRISPR-injected embryos in N-Methyllidocaine iodide (NMI) and ISA-2011B, respectively (Lee, Tardi, Man, & Choy, 1995, Semenas et al., 2014). Compared to DMSO-treated controls, embryos in which NMI enhanced PIP_2 biosynthesis showed a significant increase in the intensity of acetylated tubulin staining (Fig. 4 C) as well as in the proportion of PH3-positive cells (Fig. 4 D) on the CRISPR-injected side relative to the uninjected side. In contrast, the PIP_2 synthesis inhibitor ISA-2011B had no significant effect (Fig. 4 C, D). This indicates that the stimulation of neurite outgrowth and progenitor proliferation by Marcks and Marcksl1 is indeed PIP_2 dependent. While PIP_2 is generally thought to act upstream of PLD, additional experiments will be needed to confirm this for the developing spinal cord.

The ability of Marcks to promote PIP_2 signaling has been previously suggested to be linked to the subcellular localization of the protein, which depends on its phosphorylation status, with unphosphorylated Marcks being mostly membrane-bound and phosphorylated Marcks being largely cytoplasmic (Kim et al., 1994, McLaughlin & Aderem, 1995). In turn, the phosphorylation status of Marcks is regulated by Protein kinase C (PKC) (McLaughlin & Aderem, 1995). Although Marcks and Marcksl proteins are severely depleted in our CRISPR-injected embryos, clones of cells with at least partially functional Marcks and Marcksl proteins are expected to be present due to the mosaicism of CRISPR knockout effects in our F0 embryos. Assuming that subcellular localization of Marcks and Marcksl1 is functionally important in the spinal cord, we should thus be able to partially rescue the deficiencies of our CRISPR embryos by modulating PKC activity.

To test this hypothesis, we used the potent PKC activator Phorbol 12-myristate 13-acetate (PMA) and the broad-spectrum PKC inhibitor Go6983 (Liu & Heckman, 1998, Shen, 2003). Compared to DMSO-treated controls, embryos treated with the PKC inhibitor Go6983 showed a significant increase in the intensity of acetylated tubulin staining (Fig. 4 E) as well as in the proportion of PH3-positive cells (Fig. 4 F) on the CRISPR-injected side relative to the uninjected side. In contrast, the PKC activator PMA had no significant effect (Fig. 4 E, F). These findings suggest that the unphosphorylated, presumably membrane-bound fraction of Marcks and Marcksl1 is primarily required for neurite outgrowth and progenitor proliferation in the spinal cord. Our other findings suggest that membrane-bound Marcks and

Marcksl1 may promote these processes via the activation of PIP_2-mediated PLD signaling. However, the hierarchy of these interactions needs to be confirmed in future studies.

Expression of Marcks and Marcksl1 during spinal cord regeneration in uninjected tadpoles and after 4M CRISPR knockout

After complete transection of the spinal cord, tadpoles of *Xenopus laevis* have previously been shown to close the injury gap with cells and regenerating neurites at around ten days post transection (DPT), with almost full functional recovery at 20 DPT (Lee-Liu et al., 2014, Munoz et al., 2015, Edwards-Faret et al., 2018). Because Marcks and Marcksl1 were identified in a proteomic screen for proteins differentially upregulated after spinal cord injury (SCI) in regeneration-competent tadpoles (Kshirsagar, 2020), we next focused on the role of these proteins during spinal cord regeneration in *Xenopus*.

For these experiments, *marcks.L/S* and *marcksl1.L/S* sgRNAs (4M CRISPR) were injected into 1-cell stage embryos, which were then raised to stage 50 tadpoles (Fig. 5 A). After removing some dorsal skin, muscle, and meninges, the spinal cord was transected entirely at a mid-thoracic level. Sham-injured tadpoles were treated the same way but without transection of the spinal cord. Tadpoles were screened before SCI and at 2-, 5-, and 10-days post transection (DPT) for swimming capacity and some tadpoles at each time point were fixed, cryosectioned and evaluated by assessing the distribution of neurites (acetylated tubulin+) and measuring spinal cord gap closure length as well as percentages of proliferating cells (EdU+) and neuro-glial progenitor cells (Sox2+) (Fig. 5 A).

We first analyzed the distribution of Marcks and Marcksl1 in the uninjured spinal cord and at 2-, 5-, and 10-DPT in normal (uninjected) and 4M CRISPR-injected tadpoles. In uninjected, uninjured tadpoles, Marcks protein was detected primarily in the meningeal layer surrounding the spinal cord, with relatively little immunostaining in the spinal cord itself (Fig. 5 B-D). Barely any Marcks protein was detectable in uninjured 4M CRISPR tadpoles (Fig. 5 N, O). At 2 DPT, the levels of Marcks protein in the meninges and spinal cord remain relatively unchanged in both normal (Fig. 5 E-G) and CRISPR-injected (Fig. 5 P, Q) tadpoles. However, additional Marcks staining was observed in normal tadpoles in cells within the injury gap (Fig. 5 E-G). At 5 DPT, normal tadpoles showed an apparent upregulation of Marcks in all layers of the spinal cord adjacent to the injury site, including the ventricular zone, where neuro-glial progenitors reside, the mantle zone, which harbors differentiated neurons, and the marginal zone, occupied by neurites (Fig. 5 H-J). Marcks also

continues to be elevated in cells in the region of the injury gap, which is about to close (Fig. 5 H-J). This pattern of elevated Marcks staining was maintained at 10 DPT (Fig. 5 K-M). In contrast, 4M CRISPR tadpoles showed no significant increases of Marcks immunostaining in the spinal cord or adjacent tissues at 5- and 10-DPT (Fig. 5 R-U).

Compared to Marcks, Marcksl1 showed slightly stronger immunostaining in the spinal cord and weaker staining in the meninges of uninjected uninjured tadpoles but less pronounced upregulation after SCI (Fig. S14 A-L). As described for Marcks, Marcksl1-immunopositive cells also accumulated within the injury gap from 2 DPT onwards (Fig. S14 D-L). Again, almost no Marcksl1 immunostaining was detectable in 4M CRISPR tadpoles in and around the spinal cord before the injury, and no significant changes were observed following SCI (Fig. S14 M-T). Patterns of Marcks and Marcksl1 immunostaining for sham-operated tadpoles resembled those observed in uninjected and uninjured tadpoles and did not change at days 2-10 post-injury (Fig. S15). Taken together; these observations suggest that Marcks and Marcksl1 are present at low levels in the tadpole spinal cord but become upregulated in all layers of the spinal cord next to the injury site after SCI (in particular, Marcks), while Marcks- and Marcksl1-immunopositive cells infiltrate the lesion site.

Marcks and Marcksl are required for functional recovery after spinal cord transections in Xenopus tadpoles

To further elucidate the role of Marcks and Marcksl1 in spinal cord regeneration, we next used a behavioral test to analyze whether functional recovery after SCI is impaired in 4M CRISPR tadpoles compared to normal (uninjected) tadpoles. Tadpoles were put into 6-well plates equipped with an intermittently vibrating motor to stimulate movement and were video recorded for 1.5 minutes. Their total swimming distances were then calculated from the videos. The distances covered by uninjected and 4M CRISPR-injected uninjured tadpoles were not significantly different (Fig. 6 A). This, together with our histological data described below, suggests that while the CRISPR knockout of Marcks and Marcksl1 perturbs axon outgrowth and cell proliferation during normal development, ultimately, these tadpoles develop a relatively normally functioning spinal cord. Following SCI, there is a significant decrease in swimming distances at 2 and 5 DPT with no significant difference between uninjected and CRISPR animals (Fig. 6 A, Fig. S16 A).

However, at 10 DPT, the average swimming distance of uninjected tadpoles had recovered to a level not significantly different from pre-injury levels. In contrast, the average swimming

distance of 10 DPT CRISPR tadpoles was significantly shorter (Fig. 6 A, Fig. S16 A). Animals with sham surgeries showed no significant changes in swimming distances compared to uninjected and uninjured tadpoles over time (Fig. S16 B), suggesting that spinal cord transection alone accounts for these behavioral differences. This indicates that the CRISPR knockout of Marcks and Marcksl1 significantly delays the capacity of tadpoles to recover functionally after SCI, supporting the vital role of these proteins for spinal cord regeneration.

Marcks and Marcksl1 are required for injury gap closure and proliferation of neuro-glial progenitors during spinal cord regeneration

We next used immunostaining with acetylated tubulin and DAPI nuclear staining to analyze how Marcks and Marcksl1 knockout affects the regrowth of neurites and injury gap closure (measured as the distance between the DAPI+ ventricular zones of rostral and caudal stump) after SCI. Horizontal sections of the spinal cords of uninjured 4M CRISPR-injected animals resembled those of uninjured animals with prominent and well-distinguished ventricular, mantle, and marginal zones (Fig. 6 B, F). This demonstrates that the CRISPR-induced defects during spinal cord development described above only delay but ultimately do not prevent the formation of an adequately organized spinal cord, allowing the use of these animals for spinal cord regeneration studies.

After SCI, the length of the injury gap is initially similar for uninjected and 4M CRISPR-injected tadpoles (Fig. 6 C, G, J). However, at 5 DPT, the first axonal bridges seem to form and connect the rostral and caudal stumps in the uninjected animals, which is delayed until 10 DPT in the CRISPR tadpoles (Fig. 6 D, E, H, I). Moreover, while the injury gap decreased over time in both uninjected and 4M CRISPR-injected tadpoles, the injury gap at 5- and 10-DPT in 4M CRISPR-injected remained significantly larger than in uninjected embryos, indicating a delay in regenerative closure (Fig. 6 D, E, H, I, J).

To determine the effects of Marcks and Marcksl1 knockout on cell proliferation during spinal cord regeneration, EdU was injected into the tadpoles 16 hours before the analysis timepoint to achieve saturated labeling of the entire population of proliferating cells. DAPI-stained nuclei and EdU+ nuclei were then counted in a defined window across the injury site (i.e., the area shown in each of the panels of Fig. 7). There was no significant difference between uninjured uninjected and 4M CRISPR-injected animals (Fig. 7 A1, B1, A2, B2, I). In response to SCI, then a significant increase in the proportion of EdU+ cells was observed

in uninjected tadpoles at 2- and 5- DPT, which returned to pre-injury levels at 10 DPT (Fig. 7 A1-H1, I, Fig. S17 A). An increase in EdU+ cell numbers was seen in the ventricular zone and cells in and adjacent to the injury gap (Fig. 7 C1-F1). Sham-operated animals showed no significant changes in EdU+ cells over time (Fig. S18 B), indicating that these changes occur only after spinal cord transection. In contrast, there was no significant change in the proportion of EdU+ cells in the 4M CRISPR-injected tadpoles after SCI (Fig. 7 A2-H2, I, Fig. S17 A).

To test whether Marcks and Marcksl1 also affect the distribution and numbers of neuro-glial progenitors during spinal cord regeneration, we then visualized and quantified Sox2-immunopositive cells after SCI. Again, the distribution of Sox2+ cells in the ventricular zone was similar, and there was no significant difference between uninjured uninjected and 4M CRISPR-injected animals (Fig. 8 A1, B1, A2, B2, I).

In uninjected tadpoles at 2 and 5 DPT, we observed an increase in Sox2+ cell numbers rostral to the injury site of the transected spinal cord (Fig. 8 C1-F1). However, near the injury, Sox2+ cells were reduced (particularly at 2 DPT). This was reflected in a slight decrease in the number of Sox2+ cells counted in our standard window around the injury site (Fig. 8 I). However, at 10 DPT, Sox2+ cells were noticeably and significantly increased in the entire ventricular zone of the regenerating spinal cord, both rostral and caudal of the injury site (Fig. 8 G1, H1, I). Again, animals with sham surgeries did not show any significant changes in the population of Sox2+ cells (Fig. S18 B), indicating that the observed changes occur only after spinal cord transection.

In the 4M CRISPR-injected tadpoles, there was a slight overall decrease in Sox2+ cells at 2- and 5-DPT, similar to the uninjected tadpoles (Fig. 8 C2-F2, I). However, in contrast to the uninjected tadpoles, the CRISPR tadpoles did not show any elevation of Sox2+ immunostaining in the rostral spinal cord, and there was no overall increase in Sox2+ cell numbers at 10 DPT, with Sox2+ counts significantly decreased compared to uninjected tadpoles (Fig. 8 G2, H2, I). Taken together, our findings show that after SCI Marcks and Marcksl1 are required for multiple processes implicated in spinal cord regeneration (Lee-Liu et al., 2013, Alunni & Bally-Cuif, 2016, Rodemer et al., 2020), including neurite outgrowth and the proliferation and possibly maintenance of neuro-glial progenitors in the ventricular zone.

The PLD signaling pathway mediates Marcks and Marcksl1 functions during spinal cord regeneration

Since we found PLD signaling to be involved in mediating the effects of Marcks and Marcks1 on axon outgrowth and proliferation of neuro-glial progenitors during normal spinal cord development, we next asked whether the role of Marcks and Marcks1 for spinal cord regeneration may also be modulated by PLD activity. 4M CRISPR-injected tadpoles with spinal cord injury were exposed to the PLD activator S1P, the PLD inhibitor FIPI, or only DMSO in control embryos for seven days. At 7 DPT, the tadpoles were then compared for behavioral recovery, injury gap closure, and EdU+ and Sox2+ cell numbers (Fig. 9). The swimming recovery test revealed that tadpoles exposed to the PLD activator S1P swam significantly longer distances than control animals (Fig. 9 P). Conversely, tadpoles exposed to the PLD inhibitor FIPI traveled a shorter distance than the DMSO controls, but this difference was insignificant (Fig. 9 P). Immunostaining for acetylated tubulin combined with nuclear DAPI staining showed that injury gap length was significantly reduced in animals incubated in the PLD activator S1P. In contrast, it was significantly higher in the animals incubated in the PLD inhibitor FIPI (Fig. 9 A-C, Q). The proportion of proliferative EdU+ cells (Fig. 9 D-I, R) and of Sox2+ neuro-glial progenitor cells (Fig. 9 J-O, S) was also significantly increased in the tadpoles incubated in the PLD activator S1P and significantly decreased in those exposed to the PLD inhibitor FIPI compared to DMSO controls. Thus, in all parameters investigated, 4M CRISPR tadpoles treated with PLD activators adopted a phenotype resembling normal tadpoles after SCI. In contrast, those treated with PLD inhibitors showed more severe loss of function phenotypes than untreated CRISPR tadpoles.

This shows that PLD activation can rescue the delaying effects of Marcks and Marcksl1 knockout on functional recovery, injury gap closure, and proliferation of neuro-glial progenitors after SCI, while PLD inhibition further exacerbates them. This suggests that the functions of Marcks and Marcksl1 during spinal cord regeneration are partially mediated by PLD, similar to their roles in normal spinal cord development.

Discussion

The upregulation of Marcks and Marcksl1 proteins after SCI in the regenerating spinal cord of *Xenopus* tadpoles, but their downregulation in the non-regenerative spinal cord of froglets (Kshirsagar, 2020) led us to investigate the role of these proteins during normal spinal cord development as well as during spinal cord regeneration. Our findings indicate that these proteins act redundantly and are required for normal neurite outgrowth, proliferation, and possibly the maintenance of neuro-glial progenitor cells during spinal cord development.

However, a reasonably normal spinal cord will eventually develop after the knockdown or knockout of both proteins, suggesting that Marcks- and Marcksl1-independent mechanisms can subsequently compensate for the loss of these proteins.

We also demonstrated that Marcks and Marcksl1 play similar roles in spinal cord regeneration in tadpoles after injury. Neurite outgrowth, injury gap closure, activation of proliferation, and increase in the number of Sox2+ neuro-glial progenitors near the injury site were drastically reduced in tadpoles after the knockout of both proteins and functional recovery of swimming was delayed. The upregulation of proliferating Sox2+ cells in the ventricular zone was previously shown to be required for regeneration, suggesting that increased division and migration of these cells contribute to injury gap closure and the generation of a permissive environment for neurite regrowth (Gaete et al., 2012; Munoz et al., 2015).

Our finding that Marcks and, to a lesser extent, Macksl1 are upregulated in the entire spinal cord, including the ventricular zone, as well as in cells filling the injury gap, suggests that these proteins may act cell-autonomously in the spinal cord-derived cells to promote these regenerative processes. This is also supported by a recent single-cell RNA-seq study of regenerating *Xenopus* tails, which showed that Marcks and Marcksl1 are highly enriched in many neural cell types during tail regeneration (Aztekin et al., 2019). However, since both proteins are known to be expressed in macrophages and other immune cells and can modulate the inflammatory response (Carballo, Pitterle, Stumpo, Sperling, & Blackshear, 1999, El Amri et al., 2018; Zhou & Li, 2000), Marcks- and Marcksl1-immunopositive immune cells that infiltrate the injury site may also contribute to the regeneration-promoting effects of these proteins. Double-labeling with cell type-specific markers and single-cell RNA-seq following SCI will be required in the future to clarify the relative contribution of different Marcks- and Marcksl1-expressing cell types to spinal cord regeneration.

We also show here that a specific PLD activator can rescue deficiencies of neurite outgrowth and neuro-glial progenitor proliferation after the knockdown of Marcks and Marcksl1 during spinal cord development and regeneration. In contrast, a specific PLD inhibitor further enhances these deficiencies after SCI. Taken together with our findings that enhancement of PIP_2 synthesis and inhibition of PKC is also able to rescue the effects of Marcks and Marcksl1 knockout during spinal cord development, this is compatible with a model in which unphosphorylated, membrane-bound Marcks promotes neurite outgrowth and progenitor proliferation via PIP_2 dependent activation of PLD signaling (Fig. 9 T). This is in agreement with previous studies showing that unphosphorylated membrane-bound Marcks

promotes neurite outgrowth by modulating PIP_2 signaling due to its ability to sequester PIP_2 in membrane rafts (Laux et al., 2000), thereby potentially stimulating PIP_2 signaling (Trovo et al., 2013) but see (Laux et al., 2000). It also provides a link to previous studies suggesting an essential role of PLD-dependent mTORC1 signaling for the proliferation of neuro-glial progenitors during spinal cord regeneration (Sun & Chen, 2008, Kanno et al., 2012, Penailillo et al., 2021). However, additional experiments are needed to corroborate the various specific interactions implied by this model.

In conclusion, our present study reveals a hitherto unrecognized essential function of Marcks and Marcksl1 for spinal cord development and regeneration, highlighting the potential of *Xenopus* as a model system for regeneration studies and suggesting new pathways to be targeted for therapeutic stimulation of spinal cord regeneration in human patients.

Materials and Methods

Animals

Frogs (*Xenopus laevis*) were obtained from a commercial breeder (Xenopus One Corp, Michigan, USA). All experiments were done in accordance with Irish and European legislation under licenses AE19125/P079 and AE19125/P098 from the Health Products Regulatory Authority (HPRA).

Morpholino Antisense Oligonucleotides (MO)

Translation-blocking MOs, and a standard control MO (5′-CCTCTTACCTCAGTTACAA TTTATA-3′) were obtained from Gene Tools. *Xenopus laevis* is an allotetraploid (Session et al., 2016) and its genome contains two homeologs (denoted.L and.S, respectively) of many genes, including *marcks* and *marcksl1*. Therefore, in our functional studies, we designed MOs to block both homeologs. The marcks MO (5’-GGTCTTGGAGAATTGGGCTCCCA TT-3’) (Iioka, Ueno, & Kinoshita, 2004) target base pairs -16 to +9 of both *marcks.S* and *marcks.L*. The marcksl1.L MO (5’-GGATTCTATACTACCCATTTTCCGC-3’) targets base pairs -7 to +18 of *marcksl1.L*, while the marcksl1.S MO (5’-GGACTCTACGCTACCCATTGTGACT-3’) (Zhao, Cao, & Grunz, 2001) targets base pairs -2 to +23 of *marcksl1.S*.

The efficacy of all MOs was verified in western blots following in vitro transcription and translation (TNT-coupled Wheat Germ Extract kit, Promega) of pCMV-Sport6-marcks.S, pCMV-Sport6-marcksl1.S, and pCMV-Sport6.ccdb-marcksl1.L (1 µg/50 µl reaction) with and without MO (20 pg marcksl1.L MO or 40 pg of marcksL1.S or marcks.S MOs /50 µl reaction) as previously described (Ahrens & Schlosser, 2005). 2 µl biotinylated Transcend tRNA (Promega) was included in the reaction mix resulting in biotinylation of lysine residues. PVDF membranes were subsequently incubated with Streptavidin Alkaline Phosphatase (1:5000; Promega) to visualize proteins in Transcend Chemiluminescence Substrate (Promega). The specificity of all MOs was verified by co-injection with the rescue mRNAs (see below).

Expression Constructs

Plasmids encoding membrane-GFP (pCS2+-memGFP) and c-myc-GFP (pCMTEGFP) were provided by John Wallingford (Wallingford et al., 2000) and Doris Wedlich, respectively. cDNA clones for *Xenopus laevis* marcks.S (clone accession: BC041207), marcks.L (clone accession: BC084888), and marcksl1.S (clone accession: BC157454) were purchased from Source Bioscience, provided in pCMV-Sport6 backbone vectors and pCMV-Sport6.ccdb for *marcksl1.L*. Due to a nucleotide sequence identity of 94% between *marcks.L* and *marcks.S*, only the cDNA clone for *marcks.S* was used. All plasmids were verified by sequencing and linearized with ClaI before mRNA synthesis using the SP6 Ambion Message Machine™ Kit (Invitrogen).

For rescue experiments, chicken *marcks* (clone ID: OGa33947C) and *Xenopus tropicalis marcksl1* (clone ID: OXa00945C) ORF clones were purchased from GenScript (GenBank accession numbers: NM_001044437.1; XM_015284506.2). The clones were received in pET-23a(+) vectors, containing a His-tag and T7-tag, flanking the cloning sites on each terminal. There were 3/25 base-pair mismatches between Xl-Marcks.S MO and the pET-23a(+)-marcks_OGa33947C sequence; 9/25 mismatches between Xl-Marcksl1.L MO and pET-23a(+)-marcksl1_OXa00945C; and 10/25 mismatches between Xl-Marcksl1.S MO and pET-23a(+)-marcksl1_OXa00945C. To increase the number of mismatches between the MOs and the mRNA rescue constructs, seven and eight additional substitutions were introduced into pET-23a(+)-marcks_OGa33947C and pET-23a(+)-marcksl1_OXa00945C_plasmids, respectively, using the Q5 site-directed mutagenesis kit (New England Biolabs). These substitutions did not alter protein sequences. For mutagenesis, forward (5'-

TTTAGTAAAACAGCTGCGAAGGGCGAAGCC-3') and reverse (5'-CTGTGCACCCATGGATCCGCGACCCATTTGC-3') primers for pET-23a(+)-marcks_OGa33947C were annealed at 70 °C, while forward (5'-ATCGAGAGTAAGTCTAAGAGTGCAGATATTAGC-3') and reverse (5' GGAGCCCATGGATCCGCGACCCATTTG-3') primers for pET-23a(+)-marcksl1_OXa00945C were annealed at 63 °C. Mutagenized plasmids were verified by sequencing and linearized with AdeI before mRNA synthesis using the T7 Ambion Message Machine Kit (Invitrogen), followed by polyadenylation using the Poly(A) Tailing Kit (Invitrogen).

CRISPR/Cas9-based Gene Editing

marcks.L/S and *marcksl1.L/S* genomic sequences were derived from the most recent version of the *Xenopus laevis* genome on Xenbase (https://www.xenbase.org/) and NCBI (https://www.ncbi.nlm.nih.gov/genome/). Two single-guide RNA primers targeting the first exon of *marcks.L/S* (5'-CTAGCTAATACGACTCACTATAGGCTGCGGTCTTGGAGAATTGTTTTAGAGCTAGAAATAGCAAG-3') and second exon of *marcksl1.L/S* (5'-CTAGCTAATACGACTCACTATAGGTTGGGGTCCCCGTTGGCGGTTTTAGAGCTAGAAATAGCAAG-3'), respectively (target specific region underlined), were designed using CRISPRscan (https://www.crisprscan.org). These gene-specific sgRNA primers contained a T7 promoter site (TAATACGACTCACTATA) with five additional nucleotides in the 5' end for enhanced transcriptional output, two guanines for in vitro transcript yield efficiency, 17-18 nucleotides encoding the target-specific region (underlined), and a 23-nucleotide tail for annealing to the 80-nucleotide universal reverse primer (5'-AAAAGCACCGACTCGGTGCCACTTTTTCAAGTTGATAACGGACTAGCCTTATTTTAACTTGCTATTTCTAGCTCTAAAAC-3'). As a control, an sgRNA targeting *solute carrier family 45 member 2* (*slc45a2*) 5'-CTAGCTAATACGACTCACTATAGGTTACATAGGCTGCCTCCAGTTTTAGAGCTAGAAATAGCAAG-3'), encoding a protein that mediates melanin synthesis, was used (DeLay et al., 2018). In *X. laevis*, *slc45a2* is present as only one homeolog, *slc45a2.L*. Off-target, and editing efficiency probabilities were assessed using InDelphi (https://indelphi.giffordlab.mit.edu/), GGGenome (https://gggenome.dbcls.hp/) and CRISPRscan.

sgRNAs were synthesized (Bhattacharya, Marfo, Li, Lane, & Khokha, 2015) using PCR with Q5 High-Fidelity DNA Polymerase (NEB), 1 µM each of forward and reverse primer and the following cycling conditions: 98 °C for 30 seconds; 10 cycles of 98 °C for 10 seconds, 62 °C for 20 seconds, 72 °C for 20 seconds; 25 cycles of 98 °C for 10 seconds, 72 °C for 30 seconds; and 72 °C for 5 minutes. PCR products were purified using the DNA Clean & Concentrator-5 (Zymo Research, D4014) and in vitro transcribed using the MEGAshortscript T7 Transcription Kit (Invitrogen). After a 4-hour incubation at 37 °C and subsequent TURBO DNase treatment for 15 minutes, the sgRNA was purified using the GeneJET RNA Cleanup and Concentration Micro Kit (Thermo Scientific) in accordance with the manufacturer's protocol with the following modifications: The transcription reaction mixture was first adjusted to 50 µl with nuclease-free water, followed by the addition of 250 µl of Binding Buffer. After elution in nuclease-free water, the concentration of sgRNAs was adjusted to 500 ng/µl, and aliquots were stored at -80 °C.

Microinjections

Embryos of *Xenopus laevis* were staged according to (Nieuwkoop & Faber, 1967) and injected according to standard procedures (Sive, Grainger, & Harland, 2000). mRNAs were injected into single blastomeres at the 2- to 8-cell stage, giving rise to the dorsal ectoderm. To visualize membranes in confocal microscopy, *mem-GFP* mRNA was injected (125 pg). For the overexpression study, 100 or 300 pg of *marcks* or *marcksl1* mRNA was co-injected with 125 pg *myc-GFP* mRNA to identify the injected side. As a control, only *myc-GFP* mRNA (125 pg) was injected. Morpholinos (see above) were injected singly or as a cocktail (9 ng each) with 125 pg c-*myc*-GFP mRNA. 27 ng of the standard control MO was used in control injections. For MO rescue experiments, 300 pg mutated chicken *marcks* mRNA and 350 pg mutated *Xenopus tropicalis marcksl* mRNA was co-injected with 9 ng of each MO. For CRISPR/Cas9 experiments, embryos were injected with a ribonucleoprotein (RNP) mix containing 500 pg of each sgRNA, 1 ng TrueCut Cas9 Protein v2 (Invitrogen, A36497), and 125 pg *myc-GFP* mRNA. The RNP mix was incubated at room temperature for at least 10 min before injection.

Extraction and Analysis of Genomic DNA

Approximately five days after the injection of RNPs, genomic DNA was extracted from embryos using the Wizard Genomic DNA Purification Kit (Promega) according to the manufacturer's Animal Tissue protocol. Upon extraction, the DNA was rehydrated in 25 µl of DNA Rehydration Solution overnight at 4°C. CRISPR-targeted regions in *marcks.L/S* and *marcksl1.L/S* were PCR-amplified using the EmeraldAmp GT PCR Master Mix (Takara Bio). For every gene, each 40 µl reaction contained 20 µl of 2X EmeraldAmp Master Mix, 1 µl of the forward and reverse primer mix diluted to 10 µM, 100 ng of genomic template DNA, and PCR-grade H_2O for volume adjustment. The cycling conditions were 98 °C for 30 seconds, 30 cycles of 98 °C for 10 seconds, 60 °C for 30 seconds, 72 °C for 1 minute per kilobase of PCR product, and 72 °C for 5 minutes. The following forward (F) and reverse (R) primer pairs were used: *marcks.L* (F: 5'-ATCACCTGATGGACGCATGG-3', R: 5'-CCCCCACATCTAAAGCGGAG-3'), *marcks.S* (F: 5'-AGTGTCATGAATCAGCGGGG-3', R: 5'-GTGTGTCTATTAGCGGCGGA-3'), *marcksl1.L* (F: 5'-GCTAGGAAGAAGCGAGTCCC-3', R: 5'-ACCCGTTAACATGAGCAGCA-3'), *marcksl1.S* (F: 5'-AGAAAGAAGTGAGCCTAGAGTGATT-3', R: 5'-ATCCCTCCAAGGGTGACAGG-3'), *slc45a2.L* (F: 5'-GTTCCCTTCGCTCATACAATG-3', R: 5'-GCCAGAAAGGGGTTTATTGC-3'). 5 µl of each PCR product was run in a 1% agarose gel and the remaining 35 µls were purified using the QIAquick PCR Purification Kit (Qiagen) before being sent for sequencing (sequencing primers: *marcks.L*: 5'-CCCATGCTGTCTGTCTTTGA-3', *marcks.S*: 5'-GTGTGTCTATTAGCGGCGGA-3', *marcksl1.L*: 5'-TCTTCTTCTGGCGCCTGC-3', *marcksl1.S*: 5'-AGTTTAGGGAGGCAGGGTTG-3', *slc45a2.L*: 5'-GTTCCCTTCGCTCATACAATG-3'). Sequencing raw data from wild-type, *slc45a2*, and *marcks/marcksl1*-targeted embryos were analyzed for the frequency of insertion/deletion mutations using the Synthego ICE algorithm (https://ice.synthego.com/) (Conant et al., 2022).

Antibodies

Affinity-purified polyclonal antibodies against *Xenopus* Marcks and Marcksl1 proteins were generated by the company GenScript. For anti-Marcks, a His-tagged fusion protein with the following sequence was expressed in bacteria: MHHHHHHASPAEGEPAEPASPAEGEPAAKTEEAGSTSTPSTSNETPKKKKKRFSFKKSFKLSGFSFKKNKKENSEGAENEGA. Using the Protein BLAST NCBI tool, this immunogen (including the 6-His-tag) shared a 98.68 percent identity (E value: 3e-43) with

Marcks.L (NCBI Reference Sequence XP_018118779.1) and 98.67% (E value: 3e-42) with Marcks.S (XP_018119725.1). No other sequences in *X. laevis* (taxonomy id:8355) returned any significant alignments. The protein was purified in Nickel and Superdex 75 columns and, after LC-MS validation, was used to immunize rabbits. The antibody was then antigen-affinity-purified from sera and tested by indirect ELISA by Genscript. For anti-Marcksl1, keyhole limpet hemocyanin (KLH)-tagged peptides (CGDPKPEDPPGKQAK) were used to immunize rabbits and were affinity-purified. This peptide had a 100% sequence identity (E value: 6e-08) with both Marcksl1.L (NP_001108274.1) and Marcksl1.S (NP_001081982.2). The next closest sequence alignments returned insignificant E values greater than 0.34.

Histochemistry

Embryos and tadpoles were fixed in 4% PFA in 0.1 M phosphate buffer (PB) overnight, followed by two washes in PB for 10 minutes, before cryoprotection in 20% sucrose/PB overnight at 4°C. The specimens were then positioned in rubber forms and embedded in O.C.T. (VWR) for 30 minutes before shock-freezing in 2-Methylbutane cooled in liquid nitrogen. Immunohistochemistry on 20 µm cryosections was performed as previously described (Schlosser & Ahrens, 2004). Primary antibodies were diluted, as indicated in Table 1. The following secondary antibodies were used at 1:500 dilution supplemented with DAPI (100 ng/µl): Alexa Fluor 488- and Alexa Fluor 594-conjugated goat anti-mouse (Invitrogen A11001 and A11005, respectively); Alexa Fluor 488- and Alexa Fluor 594-conjugated goat anti-rabbit (Invitrogen A11008 and A11012, respectively); and Alexa Fluor 594-conjugated donkey anti-mouse and anti-rabbit (Invitrogen A21203 or A21207, respectively).

Incorporation and histochemical detection of 5-ethynyl-2´-deoxyuridine (EdU) was used to label the entire proliferating cell population before and after spinal cord injury. EdU was initially diluted to 5 mg/ml in 0.8x PBS, followed by 5 µl intracoelomic injections into tadpoles 16 hours before the desired time point (Edwards-Faret et al., 2017). In tadpole cryosections immunostained for Sox2, EdU was detected after secondary antibody incubation using the Click-iT™ EdU Cell Proliferation Kit for Imaging and Alexa Fluor 488 dye (Invitrogen).

In situ Hybridization

After fixation in 4% paraformaldehyde, whole-mount in situ hybridization was carried out as previously described (Schlosser & Ahrens, 2004). pcMV-Sport6-marcks.S, pCMV-Sport6-marcksl1.S, and pCMV-Sport6.ccdb-marcksl1.L were linearized with EcoRV followed by synthesis of anti-sense RNA probes using the digoxigenin RNA Labeling Kit (Sigma Aldrich) and SP6 polymerase. Vibratome sections (40 μm) were cut after the whole-mount in situ hybridization.

Pharmacological Assays

Uninjected and RNP-injected embryos (see above) were incubated in various chemical compounds three days post-fertilization for 24 hours at 14 °C in a dark incubator. All compounds were solubilized in DMSO and diluted in 0.1X MBS (Sive et al., 2000). Control embryos were incubated in 2% DMSO/0.1X MBS. The medium was changed once after 12 hours of incubation in a 12-well plate (6 embryos per well). To determine the proper dosage, a dose-titration screening was first conducted for all chemicals using dilutions of 0.01 μM, 0.1 μM, 1 μM, and 10 μM in DMSO. The highest dose that produced comparable mortality rates to the DMSO control embryos was selected for further studies. Sphingosine-1-phosphate (S1P) (1 μM, TOCRIS) and 5-Fluoro-2-indolyl des-chlorohalopemide (FIPI) (10 μM, TOCRIS) were used to activate and inhibit PLD, respectively. NMI (10 μM, TOCRIS) and ISA-2011B (10 μM, MedChemExpress) enhanced or inhibited phosphatidylinositol biosynthesis, respectively. Finally, Phorbol 12-myristate 13-acetate (PMA) (0.01 μM, TOCRIS) and Go 6983 (10 μM, TOCRIS) were used to activate or inhibit PKC, respectively.

Imaging and Statistical Analysis

Immunostained cryosections and vibratome sections were visualized using an Olympus BX51 fluorescence microscope and recorded with an Olympus DP72 camera. Some representative images were obtained by confocal microscopy (Olympus Fluoview 1000 Confocal Microscope). For each epitope, images were acquired using identical exposure settings for signal threshold determination and balancing. Representative images were flipped and/or cropped with contrast adjustments to highlight biological relevance using Image J (National Institutes of Health).

To quantify acetylated tubulin integrated density, the injected and uninjected areas of every second consecutive spinal cord section were manually selected using the freehand

selection tool and measured in ImageJ. At least eight transverse 20 µm sections were analyzed per animal, spanning the length of more than 300 µm in developing spinal cords. The integrated density for the injected and uninjected sides was averaged separately for every animal. Then, a ratio for these averages – the integrated density ratio (IDR) - was calculated for every animal. To determine Sox2/3-positive cell numbers, individual cells from at least eight alternating serial sections were counted on the injected and uninjected sides. For every animal, the ratio for the average number of cells in the injected to uninjected sides was calculated. The percentage of PH3+ cell nuclei out of all ependymal DAPI-positive nuclei was calculated for quantification of cell division on the injected and uninjected sides. For every animal, the ratio for the percentage of PH3+ cell nuclei in the injected to uninjected sides was calculated. After SCI, at least five horizontal spinal cord 20 µm sections were obtained per animal and condition. The length between the regenerating stumps was calculated using Image J, and averaged for every animal. Total cell counts from DAPI, EdU, and Sox2 images were also determined using Image J. DAPI-stained nuclei and EdU+ nuclei were counted in at least five horizontal sections per animal. Within each section, the entire population of cells in the spinal cord in a window extending 330 µm across the spinal cord and extending for 440 µm along the anteroposterior axis across the injury site and including the rostral and caudal stumps was analyzed (i.e., the area depicted in each of the panels of Fig. 7). After binary conversion and particle analysis in ImageJ, the percentage of EdU+ or Sox2+ cells over the entire nuclear cell count was calculated.

Several statistical tests were employed for this study using GraphPad Prism (San Diego, California). A one-way ANOVA was chosen to compare how a single variable, MOs or RNPs, could affect neurite outgrowth or cell proliferation. The mean of each condition was then compared using the Tukey test, which compares every mean with every other mean. For pharmacological treatments on developing embryos, a one-way ANOVA was also used with a Dunnett test to compare every mean to a control mean, which was the DMSO condition. A 2-way ANOVA was used to compare how CRISPR-gene disruption and injury time points can affect gap closure length after SCI. Here, an uncorrected Fisher's least significant difference (LSD) test was used for pairwise comparisons of two specific groups (uninjected and CRISPR) against each other at every time point. Additionally, the mean percentage of EdU+ and Sox2+ cells in CRISPR and uninjected animals were compared at different time points using a 2-way ANOVA with Sidak's test to compare every mean independently. Results are represented in box plots or bar plots indicating the range between the 25th and 75th

percentile, with all data points shown. Single data points represent the average value of a given measurement per animal, with error bars representing minimum to maximum values.

Surgery for Spinal Cord Injury

Before surgery, stage 50 tadpoles were placed in 0.1% MS222 in 0.1X MBS for approximately 30 seconds until the reflex response to touch was absent. The animals were then immobilized in a plasticine-coated petri dish and rinsed with transplantation solution (88 nM NaCl, 1 mM KCl, 1 mM $MgSO_4$ x 7 H_2O, 5 mM HEPES, 3 mM $CaCl_2$, 100 units penicillin/ml, 0.1 mg/ml streptomycin), removing any excess solution. Dorsal skin and adjacent muscle tissues from the mid-thoracic level were incised using fine forceps, exposing the spinal cord. After removing a small portion of the meninges, a tungsten wire was inserted below the spinal cord to lift it slightly, facilitating subsequent transection with a 25 gauge injection needle. For sham injury, only the skin and muscle tissues were incised. Following surgery, the tadpoles were placed in a transplantation buffer for 30 minutes before being transferred to 0.1X MBS supplemented with antibiotics (400 mg/l penicillin, 400 mg/l streptomycin, and 25 mg/l gentamicin) for the duration of the study. The animals were housed in individual wells in a six-well plate in 0.1X MBS and supplemented with antibiotics, and the media was changed twice daily for the first three days post-injury and once daily after that. Feeding the animals began two days post-surgery, consisting of sera Micron Growth Food (Sera, 00720) in 0.1X MBS. For pharmacological treatments, tadpoles were incubated post-surgery in DMSO, FIPI, and S1P, using the aforementioned concentrations, and solutions were changed once daily for seven days. Tadpoles were terminally anesthetized during the appropriate time points by prolonged exposure (20 minutes) in 0.1% MS222. Following euthanasia, the tadpoles were rinsed twice for 5 minutes in 1x PBS and fixed in 4% PFA overnight at 4°C.

Swimming Recovery Test

A quantitative recovery test was designed by recording and measuring vibration-induced swimming to analyze the recovery of tadpoles following SCI. For this, tadpoles were placed in a custom-made six-well plate attached to a 10 mm Pico Vibe vibration motor (Precision Microdrives), connected via USB to a Mega 2560 MCU Board (Arduino). The vibration's duration was programmed using Arduino’s Integrated Development Environment. Tadpoles

were placed in the recording chamber for a 1-minute equilibration period and subsequently recorded for 90 seconds, during which they were subjected to six 3-second stimulation pulses at equal time intervals. After recording, total swimming distances were measured using EthoVision XT video tracking software (Noldus) and analyzed in GraphPad Prism.

Acknowledgments

This study was funded by Science Foundation Ireland (SFI) and the European Regional Development Fund (ERDF) under grant number 13/RC/2073_P2. The authors acknowledge the use of the facilities of the Centre for Microscopy and Imaging at the University of Galway, Galway, Ireland, a facility that is co-funded by the Irish Government's Programme for Research in Third Level Institutions, Cycles 4 and 5, National Development Plan 2007–2013. During the course of this work M.E.A held a Hardiman fellowship from University of Galway and a Government of Ireland PhD Scholarship from the Irish Research Council (GOIPG/2018/500).

Competing Interest Statement: The authors have no competing interests.

Data and materials availability statement: All data are available in the main text or the supplementary materials.

References

Ahrens, K., & Schlosser, G. (2005). Tissues and signals involved in the induction of placodal Six1 expression in *Xenopus laevis*. *Dev.Biol., 288*(1), 40-59.

Alibardi, L. (2017). Biological and molecular differences between tail regeneration and limb scarring in lizard: an inspiring model addressing limb regeneration in amniotes. . *J. Exp. Zool. B (Mol. Dev. Evol.), 328*, 493-514.

Alunni, A., & Bally-Cuif, L. (2016). A comparative view of regenerative neurogenesis in vertebrates. *Development, 143*(5), 741-753. doi:10.1242/dev.122796

Aztekin, C., Hiscock, T. W., Marioni, J. C., Gurdon, J. B., Simons, B. D., & Jullien, J. (2019). Identification of a regeneration-organizing cell in the Xenopus tail. *Science, 364*(6441), 653-658. doi:10.1126/science.aav9996

Beattie, M. S., Bresnahan, J. C., & Lopate, G. (1990). Metamorphosis alters the response to spinal cord transection in Xenopus laevis frogs. *Journal of Neurobiology, 21*(7), 1108-1122. doi:10.1002/neu.480210714

Bhattacharya, D., Marfo, C. A., Li, D., Lane, M., & Khokha, M. K. (2015). CRISPR/Cas9: An inexpensive, efficient loss of function tool to screen human disease genes in Xenopus. *Developmental Biology, 408*(2), 196-204. doi:10.1016/j.ydbio.2015.11.003

Blitz, I. L., Biesinger, J., Xie, X., & Cho, K. W. (2013). Biallelic genome modification in F(0) Xenopus tropicalis embryos using the CRISPR/Cas system. *Genesis, 51*(12), 827-834.

Bock-Marquette, I., Shrivastava, S., Pipes, G. C., Thatcher, J. E., Blystone, A., Shelton, J. M., . . . DiMaio, J. M. (2009). Thymosin beta4 mediated PKC activation is essential to initiate the embryonic coronary developmental program and epicardial progenitor cell activation in adult mice in vivo. *Journal of Molecular and Cellular Cardiology, 46*(5), 728-738. doi:10.1016/j.yjmcc.2009.01.017

Brown, H. A., Thomas, P. G., & Lindsley, C. W. (2017). Targeting phospholipase D in cancer, infection and neurodegenerative disorders. *Nat Rev Drug Discov, 16*(5), 351-367. doi:10.1038/nrd.2016.252

Brudvig, J. J., & Weimer, J. M. (2015). X MARCKS the spot: myristoylated alanine-rich C kinase substrate in neuronal function and disease. *Frontiers in Cellular Neuroscience, 9*, 407. doi:10.3389/fncel.2015.00407

Carballo, E., Pitterle, D. M., Stumpo, D. J., Sperling, R. T., & Blackshear, P. J. (1999). Phagocytic and macropinocytic activity in MARCKS-deficient macrophages and fibroblasts. *American Journal of Physiology, 277*(1), C163-173. doi:10.1152/ajpcell.1999.277.1.C163

Carmichael, S. T., Archibeque, I., Luke, L., Nolan, T., Momiy, J., & Li, S. (2005). Growth-associated gene expression after stroke: evidence for a growth-promoting region in peri-infarct cortex. *Experimental Neurology, 193*(2), 291-311. doi:10.1016/j.expneurol.2005.01.004

Conant, D., Hsiau, T., Rossi, N., Oki, J., Maures, T., Waite, K., . . . Stoner, R. (2022). Inference of CRISPR Edits from Sanger Trace Data. *CRISPR J, 5*(1), 123-130. doi:10.1089/crispr.2021.0113

DeLay, B. D., Corkins, M. E., Hanania, H. L., Salanga, M., Deng, J. M., Sudou, N., . . . Miller, R. K. (2018). Tissue-Specific Gene Inactivation in Xenopus laevis: Knockout of lhx1 in the Kidney with CRISPR/Cas9. *Genetics, 208*(2), 673-686. doi:10.1534/genetics.117.300468

Edwards-Faret, G., Cebrian-Silla, A., Mendez-Olivos, E. E., Gonzalez-Pinto, K., Garcia-Verdugo, J. M., & Larrain, J. (2018). Cellular composition and organization of the spinal cord central canal during metamorphosis of the frog Xenopus laevis. *Journal of Comparative Neurology, 526*(10), 1712-1732. doi:10.1002/cne.24441

Edwards-Faret, G., Munoz, R., Mendez-Olivos, E. E., Lee-Liu, D., Tapia, V. S., & Larrain, J. (2017). Spinal cord regeneration in Xenopus laevis. *Nature Protocols, 12*(2), 372-389. doi:10.1038/nprot.2016.177

El Amri, M., Fitzgerald, U., & Schlosser, G. (2018). MARCKS and MARCKS-like proteins in development and regeneration. *Journal of Biomedical Science, 25*(1), 43. doi:10.1186/s12929-018-0445-1

Foster, D. A., & Xu, L. (2003). Phospholipase D in cell proliferation and cancer. *Molecular Cancer Research, 1*(11), 789-800.

Gaete, M., Munoz, R., Sanchez, N., Tampe, R., Moreno, M., Contreras, E. G., . . . Larrain, J. (2012). Spinal Cord Regeneration in Xenopus Tadpoles Proceeds through Activation of Sox2 Positive Cells. *Neural Dev, 7*(1), 13.

Gibbs, K. M., Chittur, S. V., & Szaro, B. G. (2011). Metamorphosis and the regenerative capacity of spinal cord axons in Xenopus laevis. *European Journal of Neuroscience, 33*(1), 9-25. doi:10.1111/j.1460-9568.2010.07477.x

Hartwig, J. H., Thelen, M., Rosen, A., Janmey, P. A., Nairn, A. C., & Aderem, A. (1992). MARCKS is an actin filament crosslinking protein regulated by protein kinase C and calcium-calmodulin. *Nature, 356*(6370), 618-622. doi:10.1038/356618a0

Iioka, H., Ueno, N., & Kinoshita, N. (2004). Essential role of MARCKS in cortical actin dynamics during gastrulation movements. *Journal of Cell Biology, 164*(2), 169-174. doi:10.1083/jcb.200310027

Kam, Y., & Exton, J. H. (2001). Phospholipase D activity is required for actin stress fiber formation in fibroblasts. *Molecular and Cellular Biology, 21*(12), 4055-4066. doi:10.1128/MCB.21.12.4055-4066.2001

Kanno, H., Ozawa, H., Sekiguchi, A., Yamaya, S., Tateda, S., Yahata, K., & Itoi, E. (2012). The role of mTOR signaling pathway in spinal cord injury. *Cell Cycle, 11*(17), 3175-3179. doi:10.4161/cc.21262

Kim, J., Blackshear, P. J., Johnson, J. D., & McLaughlin, S. (1994). Phosphorylation reverses the membrane association of peptides that correspond to the basic domains of MARCKS and neuromodulin. *Biophysical Journal, 67*(1), 227-237. doi:10.1016/S0006-3495(94)80473-4

Kshirsagar, A. (2020). *Integrated proteomic and systems biology approach to understanding injured spinal cord pathophysiology and repair.* National University of Ireland Galway, Galway, Ireland.

Laux, T., Fukami, K., Thelen, M., Golub, T., Frey, D., & Caroni, P. (2000). GAP43, MARCKS, and CAP23 modulate PI(4,5)P(2) at plasmalemmal rafts, and regulate cell cortex actin dynamics through a common mechanism. *Journal of Cell Biology, 149*(7), 1455-1472. doi:10.1083/jcb.149.7.1455

Lee-Liu, D., Edwards-Faret, G., Tapia, V. S., & Larrain, J. (2013). Spinal cord regeneration: lessons for mammals from non-mammalian vertebrates. *Genesis, 51*(8), 529-544. doi:10.1002/dvg.22406

Lee-Liu, D., Moreno, M., Almonacid, L. I., Tapia, V. S., Munoz, R., von Marees, J., . . . Larrain, J. (2014). Genome-wide expression profile of the response to spinal cord injury in Xenopus laevis reveals extensive differences between regenerative and non-regenerative stages. *Neural Dev, 9*(1), 12. doi:10.1186/1749-8104-9-12

Lee, E., Tardi, P. G., Man, R. Y., & Choy, P. C. (1995). The modulation of phosphatidylinositol biosynthesis in hamster hearts by methyl lidocaine. *Biochemical Journal, 309 (Pt 3)*(Pt 3), 871-876. doi:10.1042/bj3090871

Liu, W. S., & Heckman, C. A. (1998). The sevenfold way of PKC regulation. *Cellular Signalling, 10*(8), 529-542. doi:10.1016/s0898-6568(98)00012-6

Lu, S., Yang, L., Jiang, H., Chen, J., Yu, G., Chen, Z., . . . He, S. (2019). Bichirs employ similar genetic pathways for limb regeneration as are used in lungfish and salamanders. *Gene, 690*, 68-74. doi:10.1016/j.gene.2018.12.031

McLaughlin, S., & Aderem, A. (1995). The myristoyl-electrostatic switch: a modulator of reversible protein-membrane interactions. *Trends in Biochemical Sciences, 20*(7), 272-276. doi:10.1016/s0968-0004(00)89042-8

McLaughlin, S., Wang, J., Gambhir, A., & Murray, D. (2002). PIP(2) and proteins: interactions, organization, and information flow. *Annual Review of Biophysics and Biomolecular Structure, 31*, 151-175. doi:10.1146/annurev.biophys.31.082901.134259

McNamara, R. K., Jiang, Y., Streit, W. J., & Lenox, R. H. (2000). Facial motor neuron regeneration induces a unique spatial and temporal pattern of myristoylated alanine-rich C kinase substrate expression. *Neuroscience, 97*(3), 581-589. doi:10.1016/s0306-4522(00)00039-7

Meacci, E., Nuti, F., Catarzi, S., Vasta, V., Donati, C., Bourgoin, S., . . . Vaughan, M. (2003). Activation of phospholipase D by bradykinin and sphingosine 1-phosphate in A549 human lung adenocarcinoma cells via different GTP-binding proteins and protein kinase C delta signaling pathways. *Biochemistry, 42*(2), 284-292. doi:10.1021/bi026350a

Monovich, L., Mugrage, B., Quadros, E., Toscano, K., Tommasi, R., LaVoie, S., . . . Steed, P. (2007). Optimization of halopemide for phospholipase D2 inhibition. *Bioorganic and Medicinal Chemistry Letters, 17*(8), 2310-2311. doi:10.1016/j.bmcl.2007.01.059

Morash, S. C., Byers, D. M., & Cook, H. W. (2000). Activation of phospholipase D by PKC and GTPgammaS in human neuroblastoma cells overexpressing MARCKS. *Biochimica et Biophysica Acta, 1487*(2-3), 177-189. doi:10.1016/s1388-1981(00)00094-9

Morash, S. C., Rose, S. D., Byers, D. M., Ridgway, N. D., & Cook, H. W. (1998). Overexpression of myristoylated alanine-rich C-kinase substrate enhances activation of phospholipase D by protein kinase C in SK-N-MC human neuroblastoma cells. *Biochemical Journal, 332 (Pt 2)*(Pt 2), 321-327. doi:10.1042/bj3320321

Munoz, R., Edwards-Faret, G., Moreno, M., Zuniga, N., Cline, H., & Larrain, J. (2015). Regeneration of Xenopus laevis spinal cord requires Sox2/3 expressing cells. *Developmental Biology, 408*(2), 229-243. doi:10.1016/j.ydbio.2015.03.009

Nieuwkoop, P. D., & Faber, J. (1967). *Normal table of Xenopus laevis (Daudin)*. Amsterdam: North-Holland.

Nogueira, A. F., Costa, C. M., Lorena, J., Moreira, R. N., Frota-Lima, G. N., Furtado, C., . . . Schneider, I. (2016). Tetrapod limb and sarcopterygian fin regeneration share a core genetic programme. *Nat Commun, 7*, 13364. doi:10.1038/ncomms13364

Penailillo, J., Palacios, M., Mounieres, C., Munoz, R., Slater, P. G., De Domenico, E., . . . Larrain, J. (2021). Analysis of the early response to spinal cord injury identified a key role for mTORC1 signaling in the activation of neural stem progenitor cells. *NPJ Regen Med, 6*(1), 68. doi:10.1038/s41536-021-00179-3

Rodemer, W., Hu, J., Selzer, M. E., & Shifman, M. I. (2020). Heterogeneity in the regenerative abilities of central nervous system axons within species: why do some neurons regenerate better than others? *Neural Regen Res, 15*(6), 996-1005. doi:10.4103/1673-5374.270298

Schlosser, G., & Ahrens, K. (2004). Molecular anatomy of placode development in *Xenopus laevis*. *Dev Biol., 271*(2), 439-466.

Semenas, J., Hedblom, A., Miftakhova, R. R., Sarwar, M., Larsson, R., Shcherbina, L., . . . Persson, J. L. (2014). The role of PI3K/AKT-related PIP5K1alpha and the discovery of its selective inhibitor for treatment of advanced prostate cancer. *Proceedings of the*

National Academy of Sciences of the United States of America, 111(35), E3689-3698. doi:10.1073/pnas.1405801111

Session, A. M., Uno, Y., Kwon, T., Chapman, J. A., Toyoda, A., Takahashi, S., . . . Rokhsar, D. S. (2016). Genome evolution in the allotetraploid frog *Xenopus laevis*. *Nature, 538*(7625), 336-343. doi:10.1038/nature19840

Shen, G. X. (2003). Selective protein kinase C inhibitors and their applications. *Current Drug Targets: Cardiovascular & Haematological Disorders, 3*(4), 301-307. doi:10.2174/1568006033481375

Sive, H. L., Grainger, R. M., & Harland, R. M. (2000). *Early development of Xenopus laevis* Cold Spring Harbor, New York: Cold Spring Harbor Laboratory Press.

Sousounis, K., Bhavsar, R., Looso, M., Kruger, M., Beebe, J., Braun, T., & Tsonis, P. A. (2014). Molecular signatures that correlate with induction of lens regeneration in newts: lessons from proteomic analysis. *Hum Genomics, 8*(1), 22. doi:10.1186/s40246-014-0022-y

Stumpo, D. J., Eddy, R. L., Jr., Haley, L. L., Sait, S., Shows, T. B., Lai, W. S., . . . Blackshear, P. J. (1998). Promoter sequence, expression, and fine chromosomal mapping of the human gene (MLP) encoding the MARCKS-like protein: identification of neighboring and linked polymorphic loci for MLP and MACS and use in the evaluation of human neural tube defects. *Genomics, 49*(2), 253-264. doi:10.1006/geno.1998.5247

Su, W., Yeku, O., Olepu, S., Genna, A., Park, J. S., Ren, H., . . . Frohman, M. A. (2009). 5-Fluoro-2-indolyl des-chlorohalopemide (FIPI), a phospholipase D pharmacological inhibitor that alters cell spreading and inhibits chemotaxis. *Molecular Pharmacology, 75*(3), 437-446. doi:10.1124/mol.108.053298

Sugiura, T., Wang, H., Barsacchi, R., Simon, A., & Tanaka, E. M. (2016). MARCKS-like protein is an initiating molecule in axolotl appendage regeneration. *Nature, 531*(7593), 237-240. doi:10.1038/nature16974

Sun, Y., & Chen, J. (2008). mTOR signaling: PLD takes center stage. *Cell Cycle, 7*(20), 3118-3123. doi:10.4161/cc.7.20.6881

Sundaram, M., Cook, H. W., & Byers, D. M. (2004). The MARCKS family of phospholipid binding proteins: regulation of phospholipase D and other cellular components. *Biochemistry and Cell Biology, 82*(1), 191-200. doi:10.1139/o03-087

Szpara, M. L., Vranizan, K., Tai, Y. C., Goodman, C. S., Speed, T. P., & Ngai, J. (2007). Analysis of gene expression during neurite outgrowth and regeneration. *BMC Neuroscience, 8*, 100. doi:10.1186/1471-2202-8-100

Trovo, L., Ahmed, T., Callaerts-Vegh, Z., Buzzi, A., Bagni, C., Chuah, M., . . . Dotti, C. G. (2013). Low hippocampal PI(4,5)P(2) contributes to reduced cognition in old mice as a result of loss of MARCKS. *Nature Neuroscience, 16*(4), 449-455. doi:10.1038/nn.3342

Veldman, M. B., Bemben, M. A., Thompson, R. C., & Goldman, D. (2007). Gene expression analysis of zebrafish retinal ganglion cells during optic nerve regeneration identifies KLF6a and KLF7a as important regulators of axon regeneration. *Developmental Biology, 312*(2), 596-612. doi:10.1016/j.ydbio.2007.09.019

Wallingford, J. B., Rowning, B. A., Vogeli, K. M., Rothbächer, U., Fraser, S. E., & Harland, R. M. (2000). Dishevelled controls cell polarity during Xenopus gastrulation. *Nature, 405*(6782), 81-85.

Wohnsland, F., Schmitz, A. A., Steinmetz, M. O., Aebi, U., & Vergeres, G. (2000). Interaction between actin and the effector peptide of MARCKS-related protein. Identification of functional amino acid segments. *Journal of Biological Chemistry, 275*(27), 20873-20879. doi:10.1074/jbc.M910298199

Xu, X. H., Deng, C. Y., Liu, Y., He, M., Peng, J., Wang, T., . . . Luo, Z. G. (2014). MARCKS regulates membrane targeting of Rab10 vesicles to promote axon development. *Cell Research, 24*(5), 576-594. doi:10.1038/cr.2014.33

Yarmola, E. G., Edison, A. S., Lenox, R. H., & Bubb, M. R. (2001). Actin filament cross-linking by MARCKS: characterization of two actin-binding sites within the phosphorylation site domain. *Journal of Biological Chemistry, 276*(25), 22351-22358. doi:10.1074/jbc.M101457200

Zhang, Y., Huang, P., Du, G., Kanaho, Y., Frohman, M. A., & Tsirka, S. E. (2004). Increased expression of two phospholipase D isoforms during experimentally induced hippocampal mossy fiber outgrowth. *Glia, 46*(1), 74-83. doi:10.1002/glia.10322

Zhao, H., Cao, Y., & Grunz, H. (2001). Isolation and characterization of a Xenopus gene (XMLP) encoding a MARCKS-like protein. *International Journal of Developmental Biology, 45*(7), 817-826.

Zhou, X., & Li, J. (2000). Macrophage-enriched myristoylated alanine-rich C kinase substrate and its phosphorylation is required for the phorbol ester-stimulated diffusion of beta 2 integrin molecules. *Journal of Biological Chemistry, 275*(26), 20217-20222. doi:10.1074/jbc.M909129199

Figures

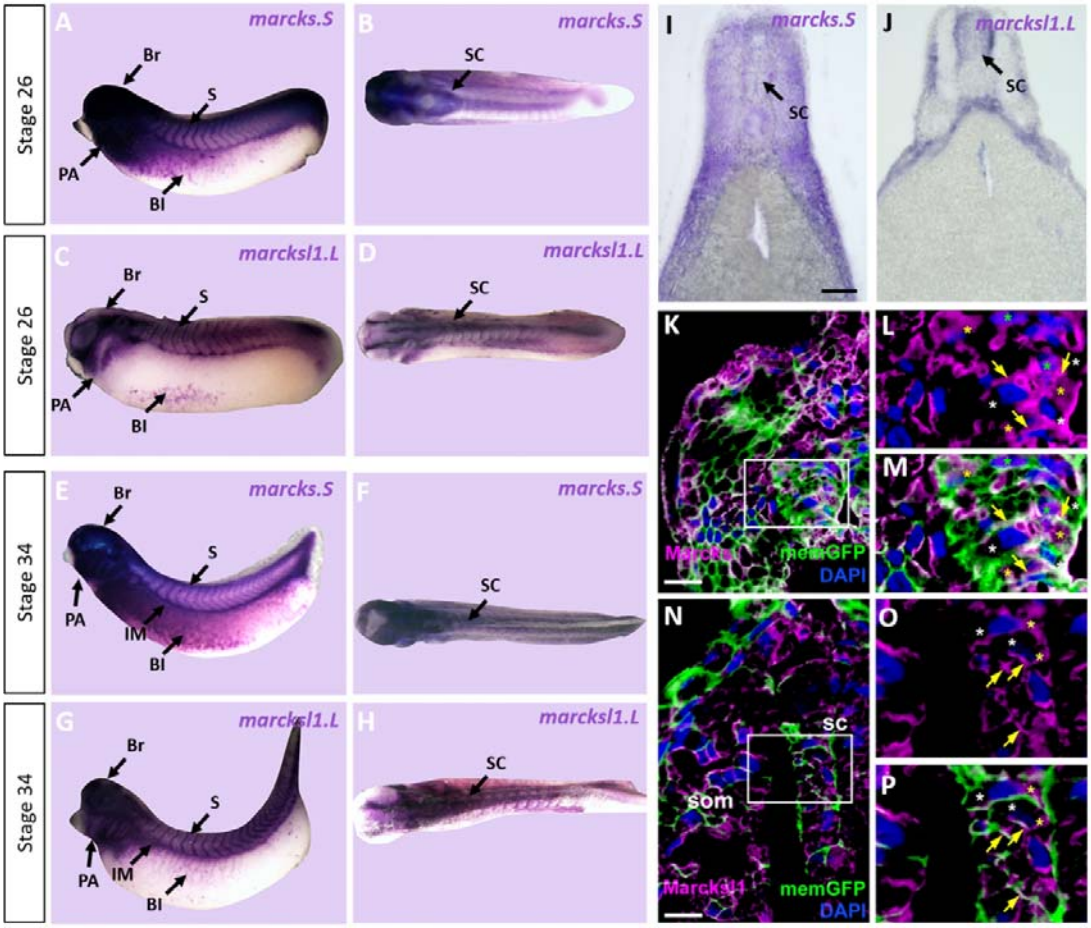

Fig. 1: Expression of Marcks and Marcksl1 in the *Xenopus* spinal cord.
A-H: Expression of *marcks.S* (A, B, E, F) and *marcksl1.L* (C, D, G, H) as revealed by whole-mount in situ hybridization in stage 26 (A-D) and 34 (E-H) *Xenopus* embryos in lateral (A,C,E,G) and dorsal (B,D,F,H) views (anterior is to the left). Expression in the spinal cord (SC), brain (Br), somites (S), intermediate mesoderm (IM), blood islands (Bl), and pharyngeal arches (PA) is indicated. I, J: Transverse sections showing expression of *marcks.S* (I) and *marcksl1.L* (J) in the spinal cord at stage 34. K-P: Immunostaining for Marcks (K-M) and Marcksl1 (N-P) protein in confocal images of transverse sections through stage 26 embryos after *memGFP* mRNA injection. White boxed areas in (K) and (N) are shown at a higher magnification in (L, M) and (N, O), respectively. Yellow asterisks indicate the expression of Marcks in the cytoplasm; green asterisks indicate expression in nuclei; white asterisks show the absence of expression in the cytoplasm; yellow arrows show expression in the membrane. Abbreviations: sc, spinal cord; som, somites. Scale bar in I = 50 µm (for I, J). Scale bar in K and N = 20 µm.

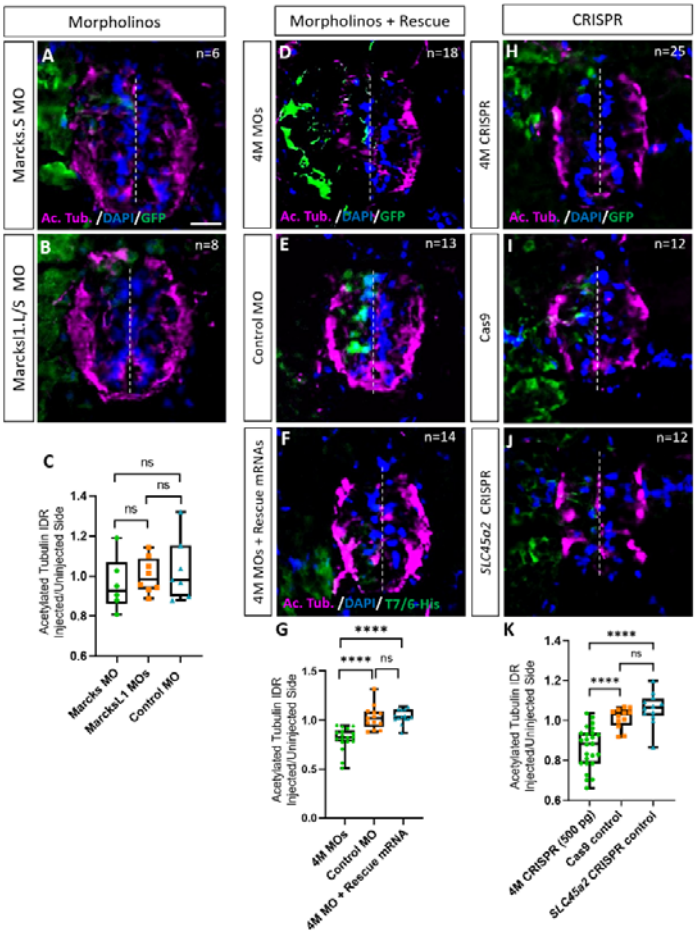

Fig. 2: Marcks and Marcksl1 are required for neurite outgrowth during *Xenopus* spinal cord development.

A-C: Evaluation of neurite outgrowth after individual morpholino (MO) knockdown of Marcks or Marcksl1 in stage 34-36 developing spinal cords. One blastomere of 4-8 cell stage embryos was injected with either 9 ng of marcks MOs (A, C), 9 ng of marcksl1.L and marcksl1.S MOs each (B, C), or 9 ng of control MO (C). All injections contained 125 pg of *myc-GFP* mRNA to identify the injected side. D-J: Evaluation of neurite outgrowth after loss of function of all four homeologs (*marcks.S*, *marcks.L*, *marcksl1.S* and *marcksl1.L)* by MO knockdown (4M MO) or CRISPR knockout (4M CRISPR). One blastomere of 4-8 cell stage embryos was co-injected with 9 ng of each MO (marcks.S, marcksl1.L, and marcksl1.S MO) (D, G); 27 ng standard control MO (E, G); 9 ng of each MO plus 300 pg of mutated chicken *marcks* and 350 pg of mutated *X. tropicalis marcksl1* rescue mRNA constructs encoding T7 and 6-His tags (F, G); 500 pg of each single-guide RNA (*marcks.L/S* and *marcksl1.L/S* sgRNA) with 1 ng Cas9 protein (H, K); 1 ng Cas9 protein (I, K); or *slc45a2* sgRNA and 1 ng Cas9 protein (J, K). All injections contained 125 pg of myc-GFP mRNA to identify the injected side. Injected (left) and uninjected (right) spinal cord sides (separated by the dashed line) were compared in transverse sections immunostained for acetylated tubulin (A, B, D-F, H-J) and for GFP, T7, and 6-His to determine the injected side. Immunostaining for acetylated tubulin was quantified (G, K) by determining the integrated density ratio (IDR) of staining in injected to uninjected sides. Significance was determined using an ordinary one-way ANOVA with Tukey's multiple comparisons test. NS, not significant; ****P<0.0001. Error bars represent minimum to maximum values showing all points with a line at the median. n refers to the number of animals analyzed. Scale bar in A = 25 µm (for all panels).

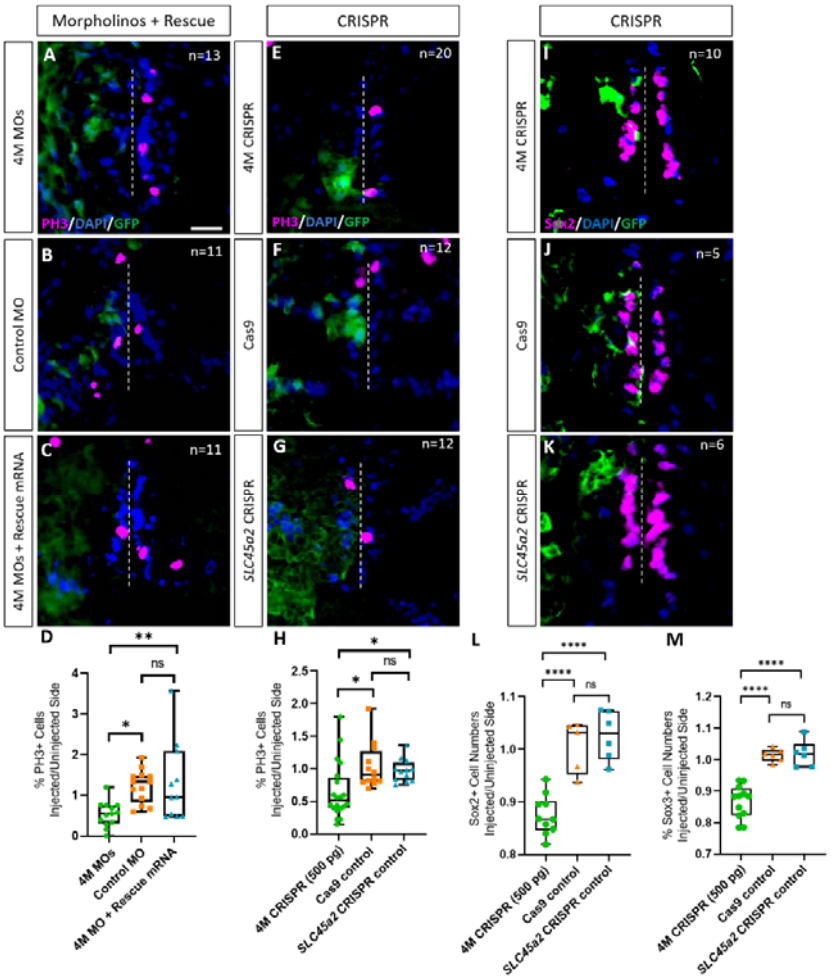

Fig. 3: **Marcks and Marcksl1 are required for the proliferation of neuro-glial progenitors during *Xenopus* spinal cord development.**

Evaluation of mitotic activity (A-H) or number of neuro-glial progenitors (I-M) after loss of function of all four homeologs (*marcks.S, marcks.L*, *marcksl1.S* and *marcksl1.L)* by MO knockdown (4M MO) or CRISPR knockout (4M CRISPR). One blastomere of 4-8 cell stage embryos was co-injected with 9 ng of each MO (marcks.S, marcksl1.L, and marcksl1.S MO) (A, D); 27 ng standard control MO (B, D); 9ng of each MO plus 300 pg of mutated chicken *marcks* and 350 pg of mutated *X. tropicalis marcksl1* rescue mRNA constructs encoding T7 and 6-His tags (C, D); 500 pg of each single-guide RNA (*marcks.L/S* and *marcksl1.L/S* sgRNA) with 1 ng Cas9 protein (E, H, I); 1 ng Cas9 protein (F, H, J); or *slc45a2* sgRNA and 1 ng Cas9 protein (G, H, K). All injections contained 125 pg of *myc-GFP* mRNA to identify the injected side. Injected (left) and uninjected (right) spinal cord sides (separated by the dashed line) were compared in transverse sections of stage 34-36 embryos immunostained for phospho-histone 3 (PH3) (A-C, E-G) or Sox2 (I-K) and for GFP, T7, and 6-His to determine the injected side. Mitotic or neuro-glial progenitor cells were quantified by determining the ratio of the percentage of PH3+ cells (D) and the numbers of Sox2+ (L) or Sox3+ (M) cells on injected and uninjected sides. Significance was determined using an ordinary one-way ANOVA with Tukey's multiple comparisons test. NS, not significant; *P<0.05; **P≤0.01; ****P<0.0001. Error bars represent minimum to maximum values showing all points with

the line at median. n refers to the number of animals analyzed. Scale bar in A = 25 µm (for all panels).

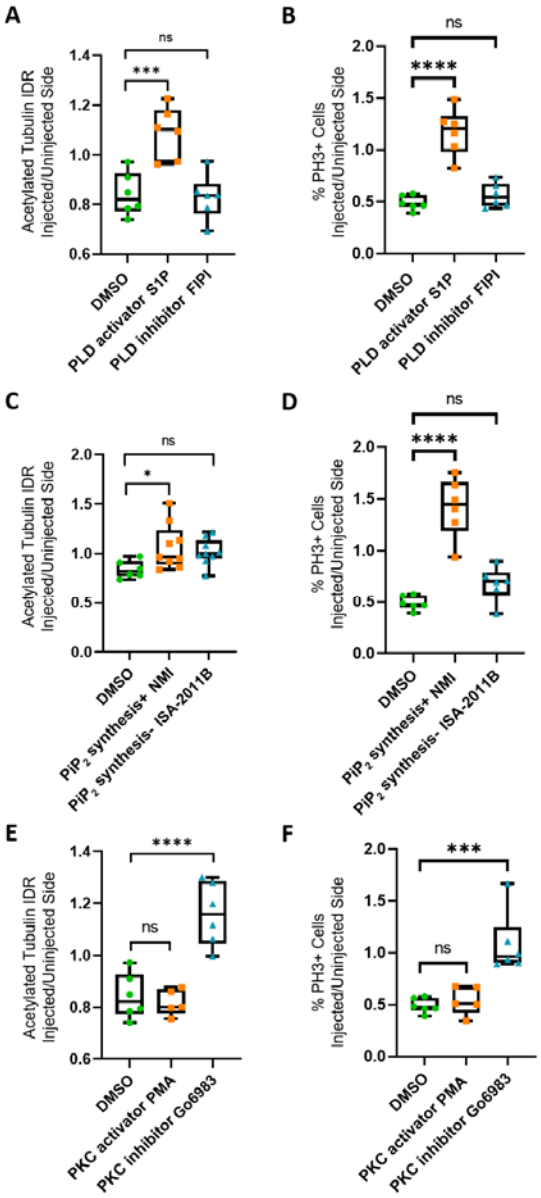

Fig. 4: Rescue of Marcks and Marcksl1 knockout phenotype by activating Phospholipase D (PLD) and other signaling pathways.

One blastomere of 4-8 cell stage embryos was co-injected with 500 pg of each single-guide RNA (*marcks.L/S* and *marcksl1.L/S* sgRNA), 1 ng Cas9 protein and 125 pg myc-GFP mRNA to knockout all four homeologs (4M CRISPR). Embryos were then incubated in compounds modulating PLD signaling (A, B), PIP_2 synthesis (C, D), or protein kinase C (PKC) activity (E, F) and analyzed for neurite outgrowth (integrated density ratio or IDR of acetylated tubulin on injected versus uninjected sides) and mitotic activity (ratio of the proportion of PH3+ cells on injected versus uninjected sides). Significance was determined using an ordinary one-way ANOVA with Dunnett's multiple comparisons test. NS, not significant; *P<0.05; **P≤0.01; ***P<0.001; ****P<0.0001. Error bars represent minimum to maximum values showing all points with the line at the median. n refers to the number of animals analyzed. Neurite outgrowth and mitotic activity was significantly increased (rescued) in the

spinal cord of 4M-CRISPR embryos by PLD activators, enhancers of PIP_2 synthesis, and PKC inhibitors. In contrast, PLD inhibitors, inhibitors of PIP_2 synthesis, and PKC activators had no effect.

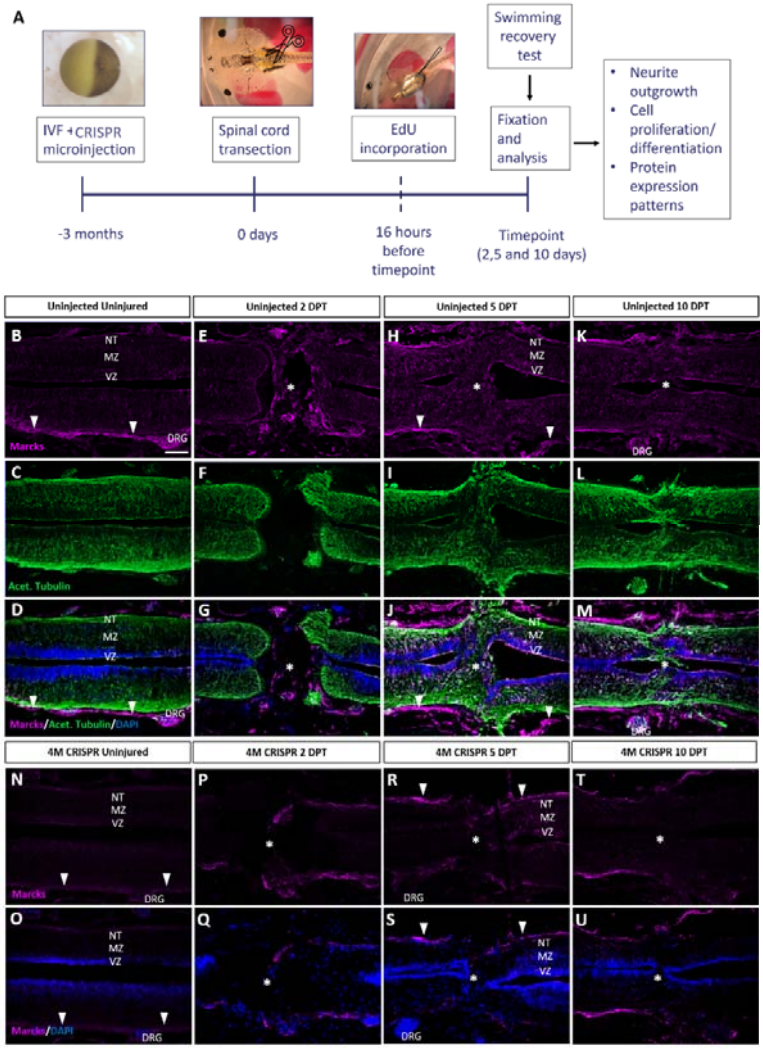

Fig. 5: Upregulation of Marcks proteins after spinal cord transection is abolished after knockout of Marcks and Marcksl1.

A: Experimental flow of the spinal cord injury study. 1-cell stage embryos were injected with CRISPR constructs targeting all homeologs of Marcks and Marcksl1. After approximately three months, the spinal cords of uninjected and CRISPR tadpoles (stage 50) were transected. Tadpoles underwent a swimming recovery test at 2-, 5-, and 10-days post transection (DPT). They were analyzed by immunostaining for regenerative outcomes, including neurite outgrowth and injury gap closure, cell proliferation (after prior EdU injection), and neuro-glial progenitor markers. B-M: Immunostaining for Marcks in horizontal sections of uninjected stage 50 tadpoles without injury (B-D) or at 2 DPT (E-G), 5 DPT (H-J), and 10 DPT (K-M). Before the injury, Marcks immunostaining was weakly detected in the ventricular zone (VZ), mantle zone (MZ), and the neurite tracts (NT) of the marginal zone of the spinal cord as well as in the dorsal root ganglia (DRG) and meninges (white arrowheads). After spinal cord transection, it was upregulated in all layers of the spinal cord cells surrounding the injury gap and in cells infiltrating the injury site (white asterisks). Scale bar = 50 µm. N=6 tadpoles per condition. N-U: Immunostaining for Marcks in horizontal sections

of 4M CRISPR-injected stage 50 tadpoles without injury (N, O) or at 2 DPT (P, Q), 5 DPT (R, S), and 10 DPT (T, U). Barely any Marcks immunostaining is detectable at any time point. N=6 tadpoles per condition. Scale bar in B = 50 µm (for all panels).

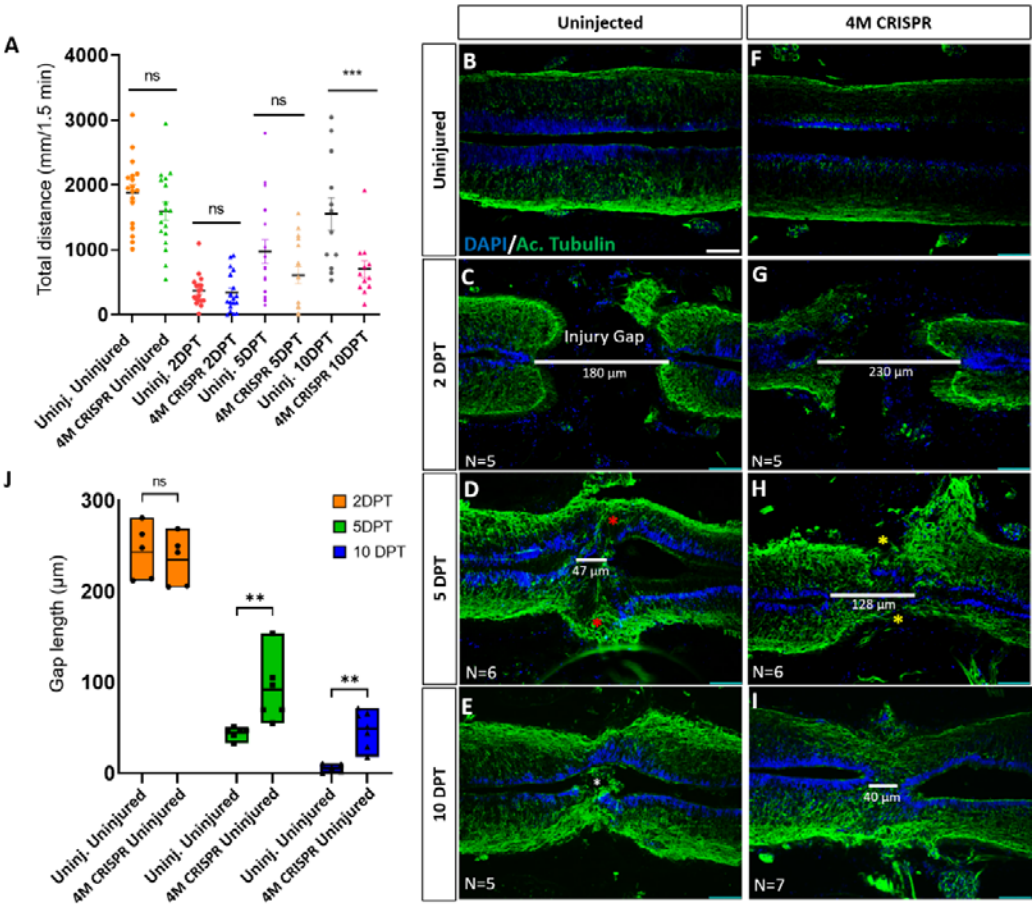

Fig. 6: Functional recovery and injury gap closure after spinal cord transection are compromised after knockout of Marcks and Marcksl1.

A: Swimming recovery test in stage 50 tadpoles after spinal cord injury. The graph shows the total swimming distance in uninjected and 4M CRISPR-injected animals before the injury and at 2-, 5-, and 10- DPT. The y-axis indicates the distance traveled by the tadpoles in millimeters for 90 seconds. Significance was determined using an ordinary one-way ANOVA with an uncorrected Fisher's least significant difference (LSD) test for multiple comparisons. NS, not significant; ***P<0.001. All data points are shown with the line at mean with SEM. Error bars represent the standard error of the mean. B-J: Comparison of injury gap closure between uninjected and 4M CRISPR-injected stage 50 tadpoles after spinal cord transection. Immunostaining for acetylated tubulin marking axonal tracts with DAPI marking nuclei in horizontal sections of the spinal cord (B-I) and quantifying injury gap length (J). Gap length was measured as the distance between the ventricular zones of rostral and caudal spinal cord stumps, as indicated by the white lines. At 2 DPT, an injury gap is visible in uninjected (B) and 4M CRISPR-injected (F) tadpoles. Axonal bridges connecting the rostral and caudal injury gap in the uninjected tadpoles at 5 DPT (red asterisks) are absent in the 4M CRISPR animals (yellow asterisks). The central canal in uninjected tadpoles becomes continuous at 10 DPT (E), in contrast to the 4M CRISPR-injected tadpoles (I). Significance was determined using a 2-way ANOVA with uncorrected Fisher's LSD of multiple comparisons. NS, not

significant; **P≤0.01. All data points are shown with the line at the mean. Scale bar in B = 50 µm (for B-H).

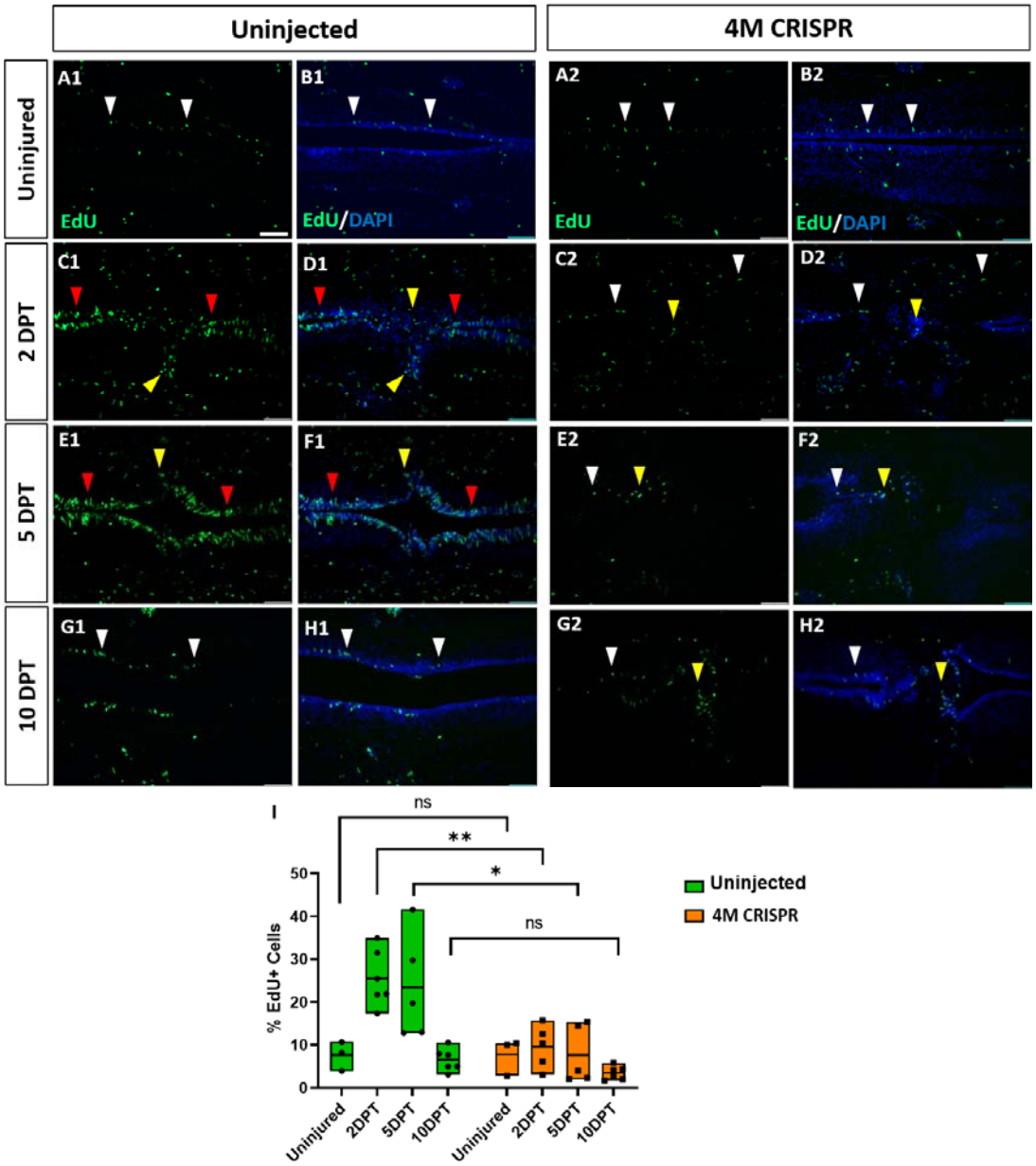

Fig. 7: Upregulation of cell proliferation after spinal cord transection is compromised after knockout of Marcks and Marcksl1.

A-H: Evaluation of EdU+ proliferative cells at 2-, 5-, and 10-DPT in horizontal sections of uninjected (A1-H1) and 4M CRISPR-injected tadpoles (A2-H2) at stage 50 (A-H) and quantification of the average proportion of EdU+ cells in a defined window of the spinal cord adjacent to the injury site (I). White and red arrowheads indicate preinjury and elevated levels of EdU+ cells in the ventricular zone, respectively. Yellow arrowheads indicate EdU+ cells in and adjacent to the injury gap. Note the increase in EdU+ cells at 2 DPT and 5 DPT in uninjected (C1-F1, I) but not 4M CRISPR-injected (C2-F2, I) tadpoles. Significance was determined using a 2-way ANOVA with Sidak's multiple comparisons test. NS, not

significant; **P≤0.01; ***P<0.001. All data points are shown with the line at mean. Scale bar in A1 = 50 µm (for all panels).

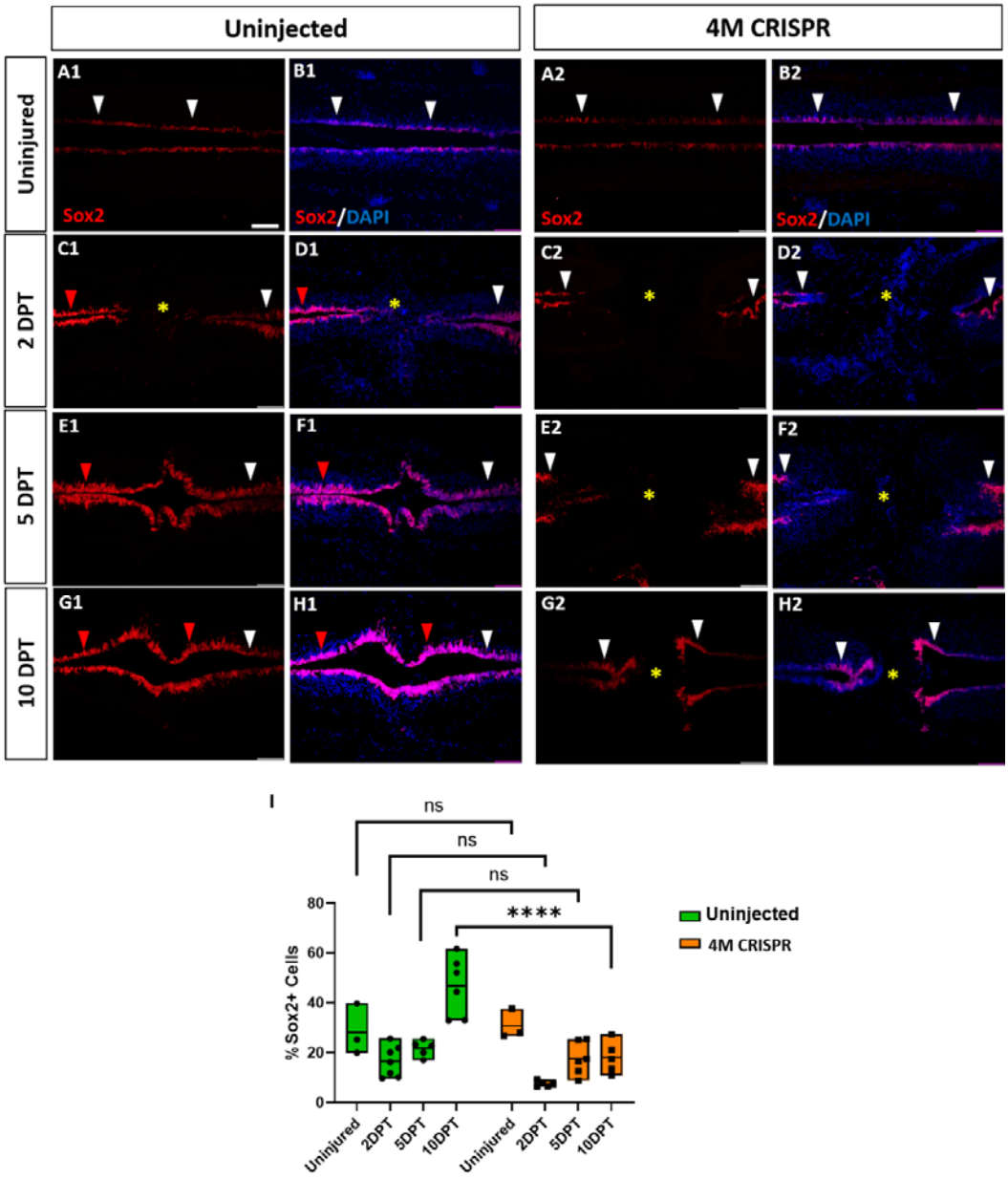

Fig. 8: Expansion of Sox2+ neuro-glial progenitors after spinal cord transection is compromised after knockout of Marcks and Marcksl1.

A-H: Evaluation of Sox2+ neuro-glial progenitors at 2-, 5-, and 10-DPT in horizontal sections of uninjected (A1-H1) and 4M CRISPR-injected tadpoles (A2-H2) at stage 50 (A-H) and quantification of the average proportion of Sox2+ cells in a defined window of the spinal cord adjacent to the injury site (I). White and red arrowheads indicate preinjury and elevated levels of Sox2+ cells in the ventricular zone, respectively. A yellow asterisk indicates the absence of Sox2+ cells in and adjacent to the injury gap. Note the increase in Sox2+ cells in the spinal cord rostral to the injury gap at 2 DPT (C1, D1) and the increase in the proportion of Sox2+ cells at 10 DPT (G1, H1, I) in uninjected but not 4M CRISPR-injected tadpoles (C2, D2, G2, H2, I). Significance was determined using a 2-way ANOVA with Sidak's

multiple comparisons test. NS, not significant; **P≤0.01; ***P<0.001. All data points are shown with the line at mean. Scale bar in A1 = 50 µm (for all panels).

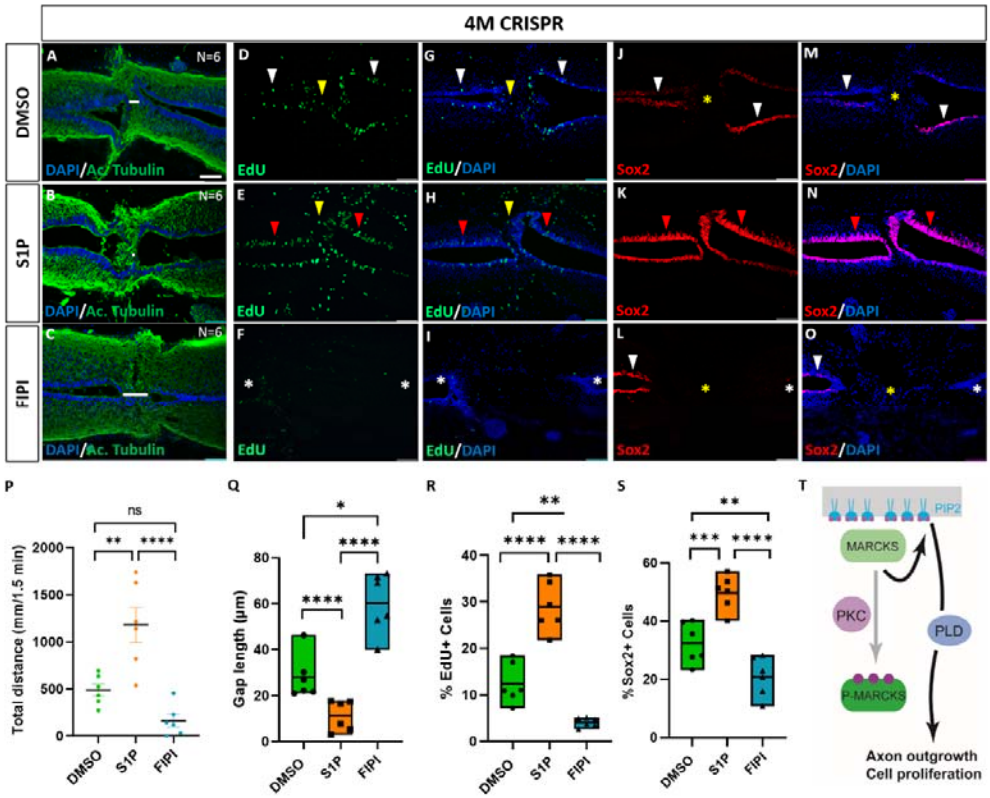

Fig. 9: Activation of Phospholipase D (PLD) signaling rescues deficiencies of spinal cord regeneration in 4M CRISPR-injected tadpoles.

A-O: Horizontal sections of 4M CRISPR-injected tadpoles at stage 50 exposed to DMSO only (controls; A, D, G, J, M) or to PLD activator S1P (B, E, H, K, N) or PLD inhibitor FIPI (C, F, J, L, O) for 7 DPT and analyzed for injury gap closure (A-C); the proportion of proliferative EdU+ cells (D-I) and proportion of Sox2+ neuro-glial progenitors (J-O). Immunostaining for acetylated tubulin and nuclear DAPI staining was used to visualize injury gap closure (A-C). Gap length was measured as the distance between the ventricular zones of rostral and caudal spinal cord stumps, as indicated by the white lines. White and red arrowheads indicate preinjury and elevated levels of EdU+ or Sox2+ cells in the ventricular zone, respectively. Yellow arrowheads indicate EdU+ cells in and adjacent to the injury gap. White asterisks indicate reduced levels of EdU+ or Sox2+ cells in the ventricular zone. A yellow asterisk indicates the absence of Sox2+ cells in and adjacent to the injury gap. P-S: Quantification of effects of pharmacological treatments in 4M CRISPR-injected tadpoles at 7 DPT on swimming recovery (P), injury gap closure (Q), proportion of proliferative EdU+ cells (R), and proportion of Sox2+ neuro-glial progenitors (S). Note that the PLD activator S1P significantly enhances swimming recovery, injury gap closure, and proportions of proliferating cells (EdU+) and neuro-glial progenitors (Sox2+) after spinal cord transection in 4M CRISPR tadpoles compared to DMSO-treated controls. At the same time, the PLD inhibitor FIPI significantly reduces injury gap closure and proportions of proliferating cells (EdU+) and neuro-glial progenitors (Sox2+). Significance was determined using an ordinary one-way ANOVA with uncorrected Fisher's LSD for multiple comparisons. N=6 animals per condition. NS, not significant; *P<0.05; **P≤0.01; ***P<0.001; ****P<0.0001. All data points are shown with the line at mean. Error bars in (P) represent the standard error of the

mean. Scale bar in A = 50 µm (for all panels). T: Model proposing that unphosphorylated, membrane-bound Marcks and Marcksl1 proteins promote axon outgrowth and proliferation during spinal cord development and regeneration in a PIP_2 and PLD-dependent manner.

Table 1 Primary Antibodies

Antigen	Company, Product Code	Reactivity	Dilution
Acetylated Tubulin	Sigma, T6793	Mouse Monoclonal	1:1000
Phospho-Histone H3 (PH3)	Merck, 06-570	Rabbit Polyclonal	1:200
GFP	Abcam, ab290	Rabbit Polyclonal	1:250
GFP	Abcam, ab1218	Mouse Monoclonal	1:250
c-Myc	Developmental Studies Hybridoma Bank (DSHB), 9E 10	Mouse Monoclonal	1:200
c-Myc	Merck, PLA0001	Rabbit Polyclonal	1:200
6-His-Tag	Abcam, ab3554	Chicken Polyclonal, FITC	1:100
T7-Tag	Invitrogen, PA1-32390	Goat Polyclonal, FITC	1:200
***X. laevis* Marcks**	Genscript, custom-made	Rabbit Polyclonal	1:200
***X. laevis* Marcksl1**	Genscript, custom-made	Rabbit Polyclonal	1:100
Sox2	Cell Signaling Technology (CST), D6D9	Rabbit Monoclonal	1:100
Sox3	Zhang et al., 2004	Rabbit Polyclonal	1:100